UNIVERSITY OF CALIFORNIA, SAN DIEGO

Nano-Structured Self-Cleaning Superhydrophobic Glass

A dissertation submitted in partial satisfaction of the

requirements for the degree Doctor of Philosophy

in

Materials Science and Engineering

by

Jin Yeol Kim

Committee in Charge:

Professor Sungho Jin, Chair
Professor Prabhaker Bandaru
Professor Jennifer N. Cha
Professor Vlado Lubarda
Professor Yu Qiao

2010

The dissertation of Jin Yeol Kim is approved, and it is acceptable in quality and form for publication on microfilm:

_____

_____

_____

_____

_____

Chair

University of California, San Diego

2010

TABLE OF CONTENTS

LIST OF FIGURES

ACKNOWLEDGEMENTS

I wish to acknowledge and deeply thank my advisor, Professor Sungho Jin for his strong encouragement, support, and direction during the course of this research. I wish to express my gratefulness to my committee members for their time and helpful suggestions: Professor Prabhaker Bandaru, Professor Jennifer N. Cha, Professor Vlado Lubarda and Professor Yu Qiao.

Chapter 2, in part, has been published in NANO, by Jin-Yeol Kim, Kunbae Noh, Chulmin Choi, Karla S. Brammer, Mariana Loya, Li-Han Chen and Sungho Jin.

I would also like to thank the following individuals for their assistance in various aspects of this work: Dr. Li-Han Chen, Kunba Noh, Chulmin Choi, Karla S. Brammer, Mariana Loya, and Young Oh. I also wish to thank Nano3 staffs: Ryan Anderson and Larry Grissom for ready to help with the fabrication processes. Special thanks to Charlotte Lauve for taking care of the administrative help for me.

I gratefully acknowledge the financial support for my doctoral program from KCC Corp. in Korea.

Finally, I wish to thank my wife, Heeyoung Chung, for her best continued support throughout my PhD study.

I also wish to thank my many friends and other colleagues who are too numerous to mention all by name.

Jin Yeol Kim

VITA

1972	Born in Youngin, Kyungki Province, South Korea
1998	B.S., Chemical Engineering, Sogang University, Seoul, Korea
2001	M.S., Chemical Engineering, Sogang University, Seoul, Korea
2010	Ph.D., Materials Science and Engineering, University of California, San Diego

SELECTED AWARDS

Awarded with the Graduate Study Abroad Scholarship by KCC for the year 2005-2010.

Awarded with pre-employee during undergraduate scholarship by Hanhwa Chemical Co. for the year 1998.

Awarded with the Dept of Chemical Engineering Fellowship,
Sogang University, Seoul, Korea for the year 1995-1997.

PUBLICATIONS

Journals Articles:

1. Superhydrophobic Glass with Engineered Surface Nanostructures and Optical Properties, J.-Y. Kim, C. Choi, K. Noh, K. S. Brammer, L. –H. Chen, and S. Jin, Langmuir (submitted)

2. Magnetic-field-guided, Microscale Partitioning of Silicon for Potential Solar Energy Applications. (in preparation)

3. Enhanced Magnetic Properties of Bit Patterned Media by Trench-Filled Nanostructure, C. Choi, D. Hong, Y. Oh, K, Noh, J. Y. Kim, L. Chen, S-H. Liou, and S. Jin, Electronic Materials Letters (submitted)

4. Long-Range Ordered Aluminum Oxide Nanotubes by Nanoimprint-Assisted Aluminum Film Surface Engineering, K. Noh, C. Choi, J.-Y. Kim, Y. Oh, K. S. Brammer, M. Loya, and S. Jin, J. Vac. Sci. Technol. B. (submitted)

5. Optically transparent glass with vertically aligned surface Al2O3 nanowires having superhydrophobic characteristics, J.-Y. Kim, K. Noh, C. Choi, K. S. Brammer, M. Loya, L.-H. Chen, and S. Jin, NANO, 5(2), 1-7 (2010)

6. 50 nm DNA Nanoarrays Generated from Uniform Oligonucleotide Films, H. Noh, A. N. Hung, C. Choi, J. H. Lee, J.-Y. Kim, S. Jin, and J. N. Cha, ACS NANO, 3(8), 2376-2382 (2009)

7. Effect of Plant Matrix and Fluid Ethanol Concentration on Supercritical Fluid Extraction Efficiency of Schisandrin Derivatives, Y, Kim, Y. H. Choi, Y.-W. Chin, Y. P. Jang, Y. C. Kim, J. Kim, J. Y. Kim, S. N. Joung, M. J. Noh, and K.-P. Yoo, J. Chromatogr. Sci., 32, 457-461 (1999)

8. Effect of plant matrices on the SFE efficiencies of schisnadrim derivatives, J. Y. Kim, and K. –P. Yoo, Theory and Applications of Chem. Eng., 5(1), 617-629 (1999)

Patents / Technology disclosures:

1. “Geometry-Defined Surface Confined Diffusion and Orthogonal DNA Interactions To Obtain Long-Range Order In Nanoparticle Arrays.” UCSD Docket No.SD2009-274-2
2. “Nanostructured Superhydrophobic, Superoleophobic and/or Superomniphobic Coating, Methods for Fabrication, and Applications Thereof” PCT/US2009/054235, 2009.
3. “The composition of biosoluble glass fiber” Korean Application No.: 2004-0030118, 2004.
4. “The composition of continuous glass fiber with high strength and elastic modulus” Korean Application No.: 2003-0015821, 2004.
5. “Biosoluble ceramic fiber composition with improved solubility in a physiological saline solution for a high temperature insulation material**”** European Patent No.: EP 1 323 687, 2002.
6. “Biosoluble ceramic fiber composition with improved solubility in a physiological saline solution for a high temperature insulation material”, Korean Patent No.: 2003-0058921, 2001.

ABSTRACT OF THE DISSERTATION

Nano-Structured Self-Cleaning Superhydrophobic Glass

by

Jin Yeol Kim

Doctor of Philosophy in Materials Science and Engineering

University of California, San Diego, 2010

Professor Sungho Jin, Chair

Superhydrophobic surfaces have received increasing attention because of their potential applications in cleantech applications such as maintaining highrise building window glasses and automobile glasses clean, consumer applications such as water-proof textiles, protective coating for telecommunication antennas, and other devices. Superhydrophobic surfaces have the self-cleaning effect, reducing the usage of energy and water required for cleaning, and minimizing pollution and waste caused by cleaning chemicals. This thesis investigates the preparation and properties of superhydrophobic glass surfaces and provides new means for fabricating these self-cleaning surfaces.

In chapter 1, the basic properties related to superhydrophobic surfaces are reviewed. In chapter 2, the fabrication of Al_2O_3 nanowires having superhydrophobic characteristics is discussed. The nanowire topography in a vertically aligned configuration was constructed by altering the geometry of as fabricated anodized

aluminum oxide pore structure through pore-widening. In chapter 3, superhydrophobic surfaces made from dry and wet etching processes were investigated. Glass nanopillar configurations with an extremely high contact angle (~ 172^{o}) were made by straightforward and economical process techniques. Optically transparent or translucent glass can be selectively made by adjusting the etching methods. In chapter 4, the morphology of diblock copolymer, polystyrene-*block*-poly (4-vinylpyridine) (PS-*b*-P4VP), is described. It is shown that gold nanoparticles embedded into a diblock copolymer selectively onto only P4VP blocks can be used as etching mask island arrays to fabricate Teflon nanopillar arrays having superhydrophobic characteristics.

New techniques for creating superhydrophobic surfaces in this work could serve as useful guidance for self-cleaning surfaces, especially window or automobile glass applications.

CHAPTER 1: Introduction

1.1 Contact angle

Understanding the behavior of water droplets on a surface is critical to understanding wettability. The interplay between the surface free energies of solid-liquid, solid-gas, and liquid-gas boundaries determines the water contact angle. Figure 1 schematically illustrates the contact angle behavior on smooth surfaces. If the contact angle is less than 90º, the surface wetting is thermodynamically more favored and the surface is defined as a hydrophilic surface. If the dry surface is more favored, then the surface is made hydrophobic, with its contact angle generally greater than 90º. The contact angle on the smooth surface can be calculated by Young's equation:

$$\cos\theta = \frac{\gamma_{sv} - \gamma_{sl}}{\gamma_{lv}} \tag{1}$$

, where γ_{SV}, $\gamma_{SL \text{ and }}\gamma_{LV}$, denotes the surface tension energy per unit surface of the solid-vapor, solid-liquid, and liquid-vapor interface, respectively.

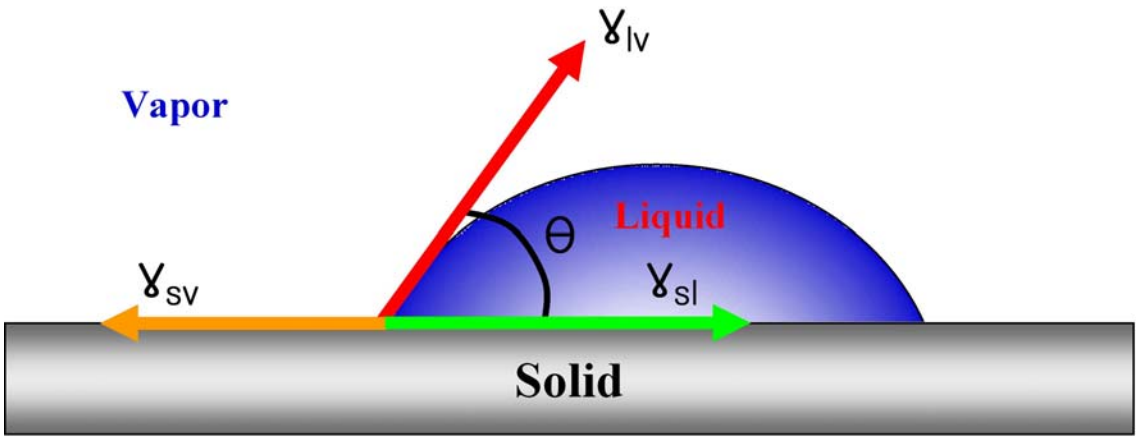

Figure 1. The contact angle on the smooth surface.

Wettability in reality is more complex, and the contact angles cannot be expressed by a simpleYoung's equation because it assumes that the surface is perfectly smooth, which is often not true on real surfaces. The apparent contact angle on a rough surface can be expressed by Wenzel and Cassie-Baxter models. [1, 2] The Wenzel model assumes that the liquid fills up the grooves on a rough surface, which is the homogeneous wetting, or noncomposite wetting, as seen in Figure 2, and is defined by the equation (2) for the contact angle on a rough surface. In this model, "roughness factor" designated by r, the ratio between the true and the geometric surface, is introduced to correct Young's equation.

$$\cos\theta_W = r\cos\theta_S \tag{2}$$

where r is the roughness factor, and θ_S is the intrinsic contact angle on the smooth surface.

In the Cassie-Baxter model, which is also called "the air pocket model", the presence of the two-phased surface is assumed, with one of the phases being air and the other being the solid material. This represents a situation of air trapped below the water drop. This model describes the apparent contact angle on a composite surface, which is heterogeneous wetting state. The Cassie-Baxter model is represented by the equation (3):

$$\cos\theta_c = f_1\cos\theta_1 + f_2\cos\theta_2 \tag{3}$$

where θ_c is the apparent contact angle of the liquid droplet, f_1 and f_2 are the projected area fraction of phase 1 and phase 2, respectively. The angle θ_1 and θ_2 are the equilibrium contact angle of the droplet contact angles of the droplet on flat surface

of the phase 1 and phase 2 materials, respectively. Since the water contact angle θ_2 in air is 180º (non-wetting), $\cos\theta_2 = -1$. Together with the relationship of $f_1 + f_2 = 1$, equation (3) becomes:

$$\cos\theta_c = f_1(\cos\theta_1 + 1) - 1 \tag{4}$$

If f_1 is very small, like a sharp needle array, there will be a lot of air under the water droplet, and $\cos\theta_c$ can approach -1 with the water contact angle θ_c becoming close to 180º.

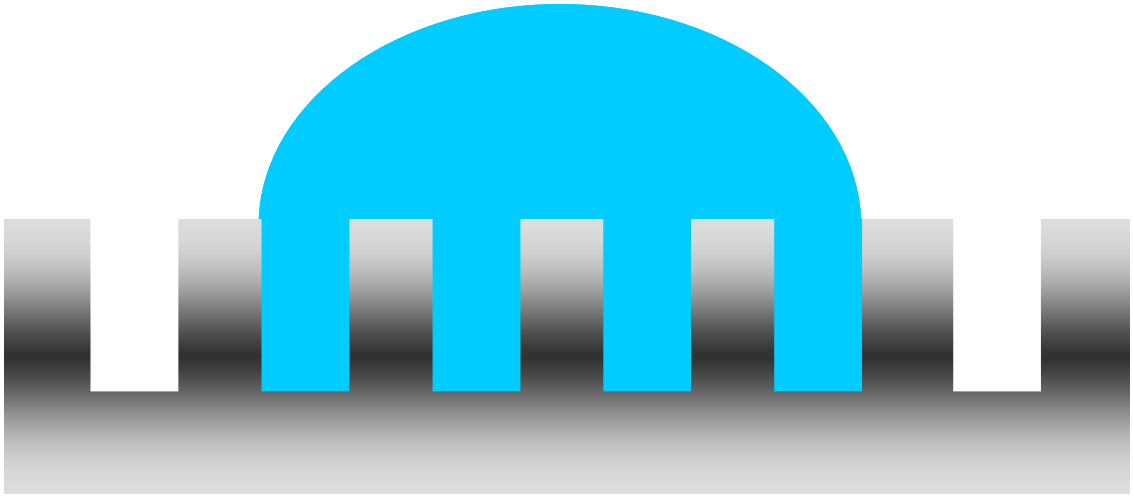

Figure 2. Contact angle on a rough surface in Wenzel's model.

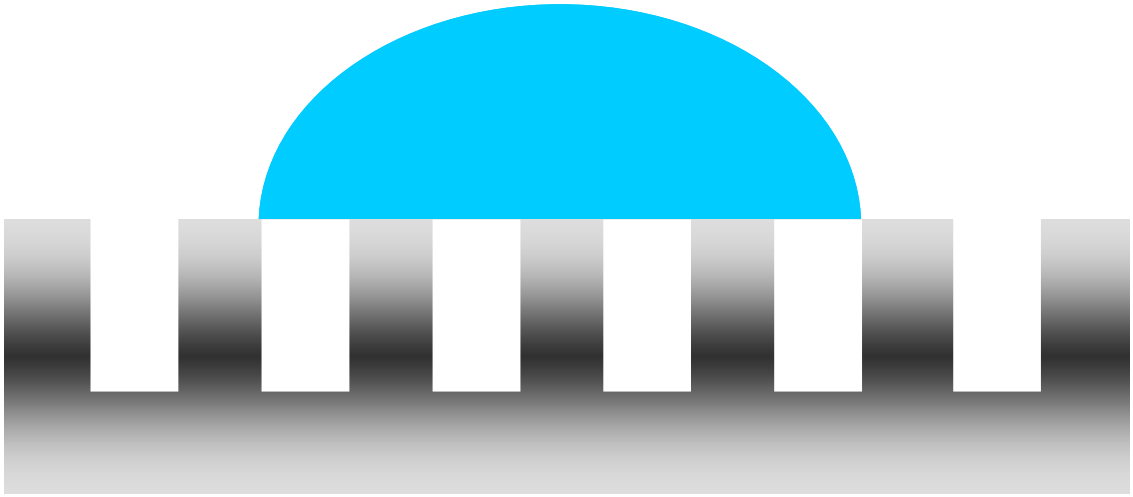

Figure 3. Contact angle on a rough surface in Cassie-Baxter model.

1.2 Self-cleaning effect

The Lotus flower is considered a symbol of purity in the some Asian religions presumably due to the water-nonwetting and self-cleaning characteristics of its leaves. The leaves remain relatively clean without dirt even when emerging from muddy waters or when they unfold. This characteristics of self-cleaning and high water-repellency was discovered in 1977 by the botanists Barthlott and Neihuis.[3] By analyzing the structure, they discovered that the surface of the lotus leaves which showed a combination of nano- and micro-structures as shown in Figure 4. A microstructure covered with nanoscale wax crystals is seen. The combination of the chemical property of wax and two different levels of roughness causes self-cleaning on the leaves of the Lotus, with the contact angle often being larger than 150º. The study of superhydrophobic phenomenon is inspired by the observation of Lotus effect.

A droplet on the inclined surface of the lotus leaf rolls over the contamination on the surface, and the particle is then removed from the surface like seen in Figure 5. The particles are easily removed from the surface due to the small contact area of the leaf and particles.

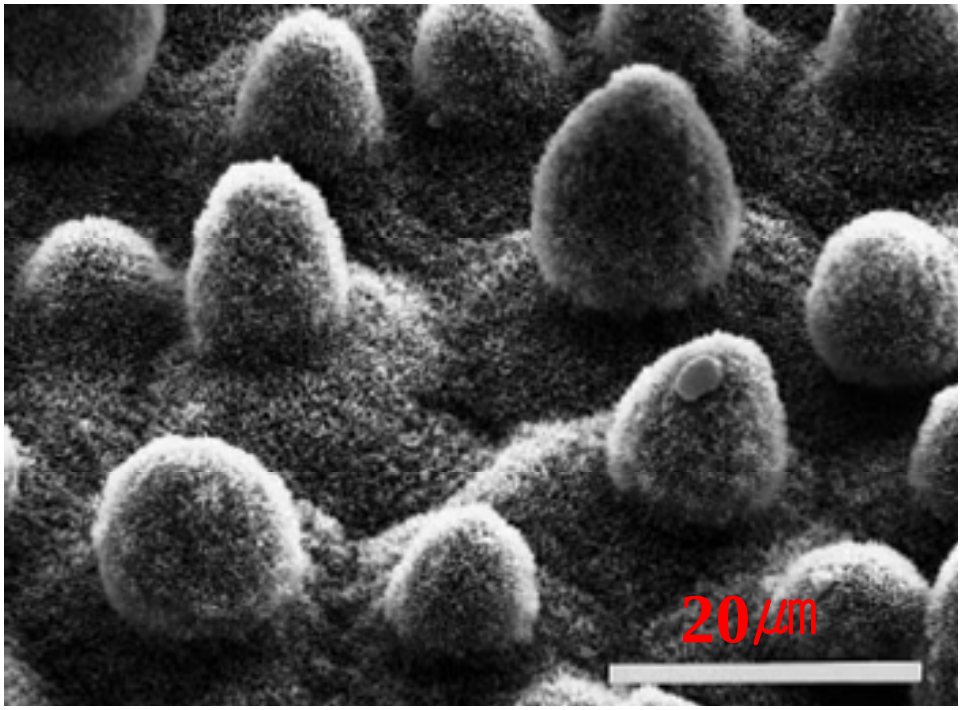

Figure 4. SEM image of the lotus leaf. The microstructure covered with nanoscopic wax crystals.[3]

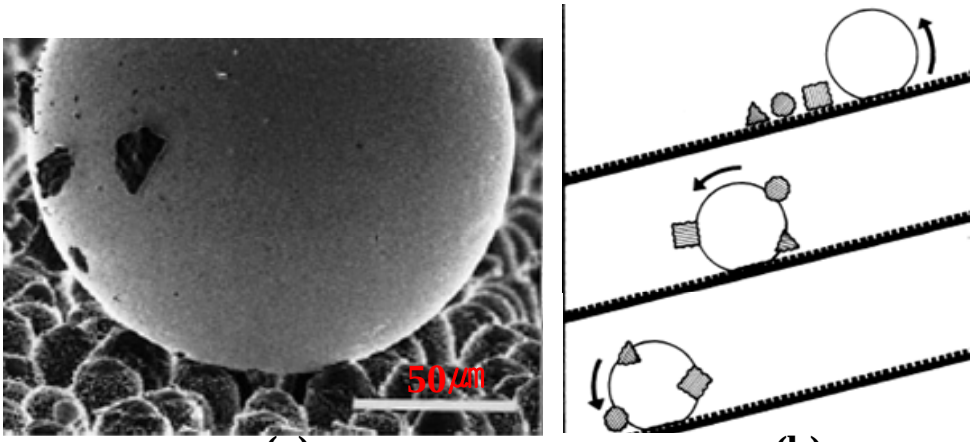

Figure 5. The image of the droplet on the leaf surface and diagram of self-cleaning. (a) Mercury droplet on the leaf surface of Colocasia esculenta, demonstrating the Lotus-Effect, and (b) Diagram summarizing the process of self-cleaning.[3]

1.3 Surface coating

The wettability of a surface is affected by two different factors, the chemistry and topography of the surface. Typically, if the contact angle of the droplet on a flat surface is greater than 90^o (hydrophobic), roughening the surface will result in an apparent contact angle greater than contact angle on a flat surface, often leading to a superhydrophobic state. On the contrary, if the contact angle of a flat surface is less than 90^o (hydrophilic), then the apparent contact angle of roughened surface often becomes much less than the contact angle of a smooth surface, sometimes leading to superhydrophilic state. [4]

To obtain superhydrophobic surfaces, a hydrophobic coating is required on the surface in order to reduce the surface energy. To lower the surface energy of the surface, fluoroalkylsilane (FAS),[5-8] trichlorosilane with fluorocarbon chains,[9-11] poly(tetrafluoroethylene)(PTFE),[12] and fluoropolymer plasma step[13] have been reported. One of the most frequently used chemicals is a fluorinated self-assembled monolayer (SAM) with $–CF_3$ terminations, and perflourinated chains have a surface free energy of 6.7 mJ/m^2.[14] Figure 6 shows the schematic diagram of fluorinated self-assembling monolayer process on the surface which is covalently bonded with oxide on the surface.[15]

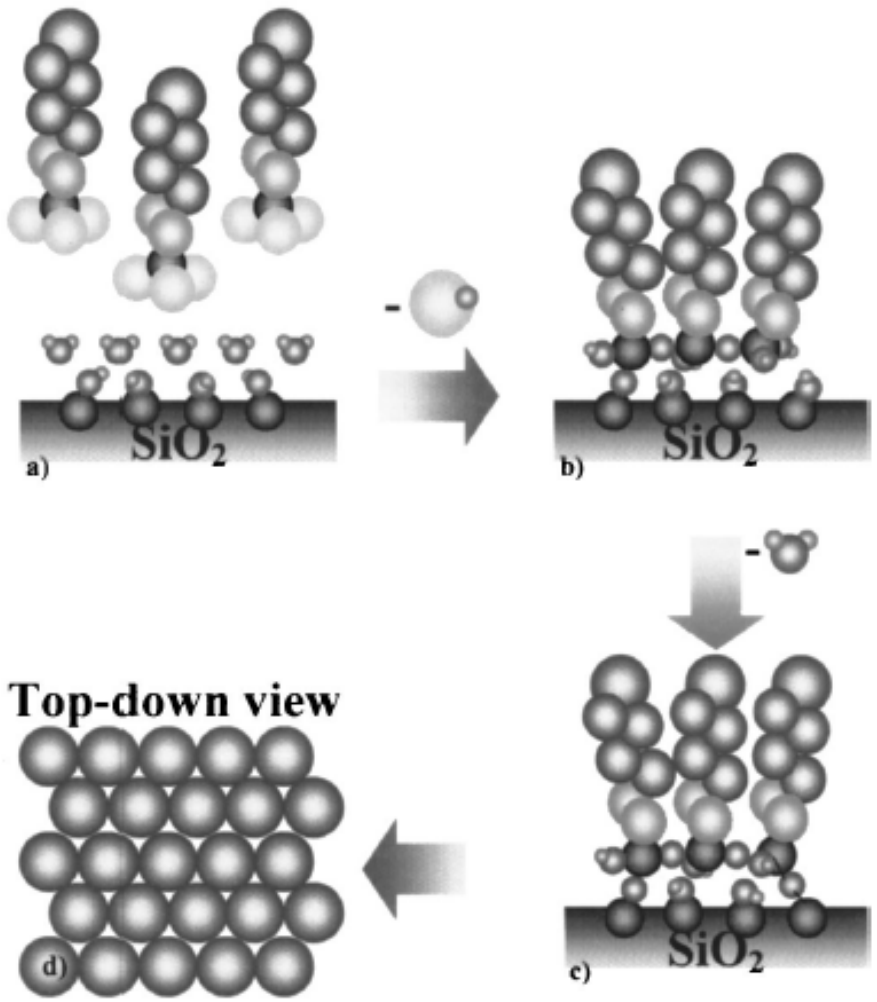

Figure 6. The schematic diagram of a fluorinated self-assembling monolayer.[15]

1.4 Thesis Outline

In this thesis work, we have developed a practical device fabrication technique to impart superhydrophobic characteristics to glass surfaces. This thesis investigates the characteristics and morphologies of superhydrophobic surfaces. We have addressed practical application perspectives. The nano-structure surfaces with high contact angles created in this work could be useful for applications requiring self-cleaning surfaces such as building window glasses, and automobile glasses.

Chapter 1 gives brief backgrounds related with superhydrophobic surfaces including contact angle, property of self-cleaning effect, and surface coating.

Chapter 2 discusses the fabrication of Al_2O_3 nanowires having superhydrophobic characteristics made by altering the geometry of as fabricated anodized aluminum oxide structure through pore-widening.

Chapter 3 contains superhydrophobic glass made from dry and wet etching processes, and discusses that optically transparent or translucent glass can be selectively fabricated by etching methods.

Chapter 4 demonstrates the morphology of polystyrene-*block*-poly (4-vinylpyridine) (PS-*b*-P4VP) copolymer. Gold nanoparticles embedded into only P4VP blocks can be used as etching masks to create Teflon nanopillar arrays having superhydrophobic characteristics.

Chapter 5 gives a summary of the main results in the work, and what needs to be done in the future.

The following papers have been included in the thesis:

1. J.-Y. Kim, K. Noh, C. Choi, K. S. Brammer, M. Loya, L.-H. Chen, S. Jin, “Optically Transparent Glass with Vertically Aligned Surface Al2O3 Nanowires Having Superhydrophobic Characteristics”, NANO, Vol. 4, No. 2, 2010 (In press)
2. J.-Y. Kim, C. Choi, K. Noh, K. S. Brammer, M. Loya, L.-H. Chen, S. Jin, “Superhydrophobic Glass Engineered Surface Nanostructures and Optical Properties”, Langmuir (submitted)

CHAPTER 2: Optically Transparent Glass with Vertically Aligned Surface Al_2O_3 Nanowires Having Superhydrophobic Characteristics

In this section of the thesis research, the self-ordered pore structure of anodic aluminum oxide (AAO) has been utilized to fabricate superhydrophobic glass as a basis to conveniently form large-area Al_2O_3 nanowire arrays on a glass surface. An aluminum oxide nanowire array has been produced by aluminum film deposition on glass followed by anodization to form vertical pore arrays, then with additional, controlled chemical etching. The glass surface so prepared is highly superhydrophobic, with a contact angle as high as 169º. The thinness (~340 nm) and vertical alignment of the aluminum oxide nanowires with empty spaces in-between essentially contribute to maintaining the optical transparency of the glass substrate. Interestingly, substantially suppressed UV transmission in the ~300 – 400 nm spectrum region was observed with the presence of the Al_2O_3 nanowires on the glass substrate. Such a durable surface ceramic nanowire structure can be useful for producing superhydrophobic, self-cleaning glasses with a variety of potential applications such as UV protecting glass windows for high rise buildings with reduced consumption of water and cleaning chemicals for positive environmental effects.

2.1 Introduction

The water-repellent characteristics of the lotus effect[3] or superhydrophobicity, has become a subject of great scientific and technological interests in recent years, for example, with potential applications as self-cleaning surfaces. The native surface of the lotus flower leaves has an unusual topography, with a unique combination of microscale

and nanoscale structures that cause water to form almost spherical droplets when in contact with the surface. When a water droplet is placed, it neither wets nor adheres onto such a superhydrophobic surface but simply rolls away carrying dust and dirt, acting as a natural cleaning mechanism. Several methods have been adopted to fabricate a superhydrophobic surface which is defined by its contact angle (CA) of water droplets in excess of ~150˚. There are many different techniques used to fabricate superhydrophobic surfaces with protruding nanostructures for mimicking the lotus topography, such as formulating two different scales of roughness,[16-18] utilizing template fabrication,[19] the use of fibers,[20, 21] phase separation,[22, 23] crystal growth,[24] chemical etching,[25] and applying a plasma-deposition method.[26] Potential applications of superhydrophobic surfaces range from self-cleaning building exteriors, window glasses, automobile windshields, and water-proof textiles.

Anodic aluminum oxide (AAO) has been used as one of the most popular periodic templates to fabricate nanodots[27, 28] and nanowires[29-34] for potential applications in magnetic and electronic devices as well as optoelectronic structures. Recently, the AAO template has been used for filling of polymers and subsequent removal of the AAO matrix to fabricate polymeric wire arrays with superhydrophobic characteristics.[16, 19, 35]

In this research, the anodized aluminum oxide (AAO) pore structure has been used as the base coating material on a glass substrate. On the AAO coating, a chemical etching was employed next for the conversion of the aluminum oxide nanopore configuration into nanowire shapes to impart a superhydrophobic surface characteristics with the contact angle approaching ~170º, which is superior to many known

superhydrophobic coatings. Such a ceramic based self-cleaning surface is also highly desirable as it is much more durable and wear-resistant than mechanically weak polymer type coatings. The reduced UV transmission can also be useful for some self-cleaning glass window applications.

2.2 Superhydrophobic glass fabrication

2.2.1 Materials and fabrication

Glass microscope slides (Fisher Scientific, Fisherfinest) and Si wafers with p-type <100> (Ultrasil Corporation) were used as substrates for the experiments. For fabrication of the aluminum oxide nanopore samples and subsequent nanowire samples, 400nm-thick Al film (with a triple underlayer structure of 20 nm thick Ti adhesion layer + 30 nm thick Au + 10 nm thick Ni layer) was sputter-deposited on the silicon using a Nor-Cal sputter system at a base pressure of 2×10^{-7} torr. On the glass substrate, the Al film coating was done without a triple underlayer structure. Prior to anodization, backside and edges of the Al film on the substrate were coated with an insulating lacquer (Tolber Division Inc., Microshield) in order to minimize/reduce local nonuniform current distribution on the Al film surface to be anodized. Anodization was performed at 5^{o}C at 25V in 0.3M oxalic acid solution with magnetic stirring using a DC power supply (HP 3612A). The controlled, partial chemical etching of the AAO layer to induce pore widening and produce aluminum oxide nanowire array was accomplished by placing the AAO coated glass substrate in a bath containing 0.51M phosphoric acid solution for various time periods.

2.2.2 Hydrophobic coating

Hydrophobic surface coating of the nanowire structure for enhanced superhydrophobicity was achieved by a fluoroalkylsilane (FAS) type coating of (heptadecafuorodecyl-1,1,2,2-tetrahydrodecyl) trimethoxylsilane (with a formula of $CF_3(CF_2)_7CH_2CH_2Si(OCH_3)_3$, procured from Gelest, Inc., No. SIH5841.5). The FAS solution was prepared as 1 wt. % in methanol solution. After finishing a chemical etching of AAO in a phosphoric acid solution for pore widening and eventual nanowire formation, the samples were rinsed immediately with de-ionized water, immersed into the FAS solution at room temperature for 2 h, and subsequently heated at 130°C for 1h. For the supercritical CO_2 drying to untangle the agglomerated nanowires, a critical drying machine (Electron Microscopy Science, EMS 850 critical point drier) was used. The samples coated with FAS coating were placed in the critical dry chamber, and subsequently washed 3 times with liquefied CO_2, and followed by supercritical dry at 90 bar pressure and 37°C. After critical dry, the samples were heated at 130°C for 1h.

2.2.3 Sample characterization

The microstructure of the processed Al_2O_3 nanowires specimen was examined by using a field emission scanning electron microscope (FE-SEM: Phillips, XL30 ESEM). The optical transmittance of the sample was measured with a spectrophotometer (Varian Inc., Cary 500). Water droplet contact angles of the samples were measured with the sessile drop method with Video Contact Angle System (KSV Instrument Ltd., CAM100) containing analysis software (Figure 7). Instead of a macro-pipette, we prepared and used a micropipette/needle with less surface area in order to

facilitate the measurement of contact angles because it was very difficult to transfer the water droplet from a typically hydrophilic pipette onto a very hydrophobic sample surface with high contact angles. Such a micropipette was fabricated from a quartz capillary tube (1.0 mm outside diameter and 0.7 mm inside diameter) by using a pipette maker (Sutter Instrument Co., P-2000), followed by a hydrophobic coating of the micropipette surface, which allowed an easy transfer of the droplet to the sample surface.

Figure 7. Image of contact angle gonimeter.

2.3 Results and Discussion

It is well known that an improved ordering of nanopores in the AAO template is obtained by using a two-step anodization process.[31, 36] However, a single-step anodization approach has been used for simplicity of processing, as superhydrophobic surfaces do not necessarily have to have a well-ordered periodic structure. For fabrication of aluminum nanowire array, an aluminum film (~400 nm thick) was first deposited on glass surface by DC sputter deposition process, followed by the anodization treatment. The pores of AAO are then widened by chemical etching. Figure 8 schematically illustrates the concept of aluminum oxide nanowire fabrication from the AAO nanopore structure. During etching, neighboring pores become larger (Figure 8(b)), eventually meet with each other, and the remaining pseudo-triangular regions become nanopillar or nanowire arrays (Figure 8(c)).

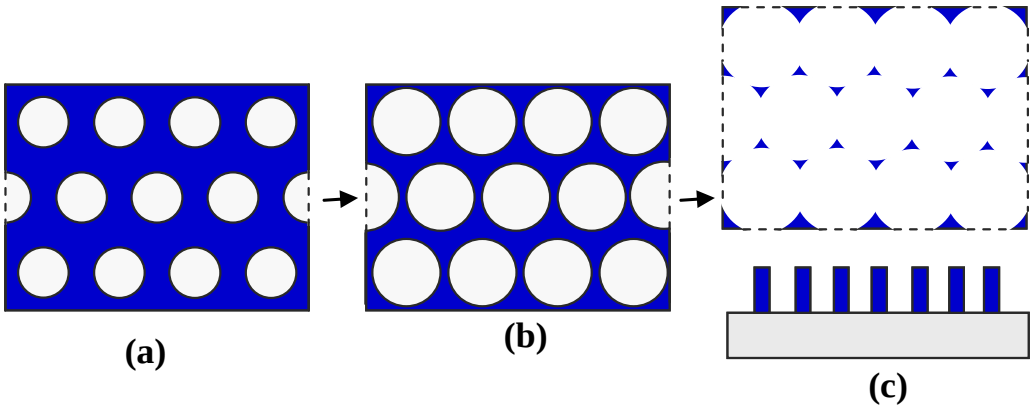

Figure 8. Schematic illustration of the formation of alumina nanowires. (a) AAO template on a substrate, (b) Enlargement of pore size by a chemical etching process, and (c) The formation of alumina nanowires, top and cross section views.

Presented in Figure 9 are SEM images of the AAO structure and the evolution of microstructure during various stages of chemical etching. The as-anodized AAO structure prepared at 25V exhibited an average pore diameter of ~20 nm as shown in Figure 9(a). The AAO sample was then subjected to chemical etching by placing in a 0.51M phosphoric acid (H_3PO_4) solution. As shown in Figures. 9(b)-(d), the pore diameter increases with increasing etching time. After 20 minute etching, the pore diameter becomes ~32 nm average (Figure 9(b)), which increases further to 49 nm after 40 minute etching (Figure 9(c)). Upon further etching, for up to 55 minutes, results in a nanowire formation, with an average diameter of ~30-40 nm and a height of ~340 nm.

Even longer etching period of 65-70 minutes led to a further reduced nanowire diameter of ~20 nm as shown in Figs. 10(a)-(c). With continued etching, for example for 80 minutes or longer, the nanowires break and become loose to be detached from the substrate surface. The alumina nanowire layer is completely etched away with an etching time over 90min.

For generally finer nanowire diameters of ~30 nm or smaller, aqueous processing followed by air drying tends to get the nanowire agglomerated, presumably due to the advancing liquid-vapor interface as shown for Figs 10(a) and (b). In order to minimize such agglomeration of nanowires on drying, we employed a supercritical CO_2 drying method. This resulted in a significantly improved nanostructure with much more separated Al_2O_3 nanowires (Fig. 10(c)), and ultimately improved (more hydrophobic) contact angle.

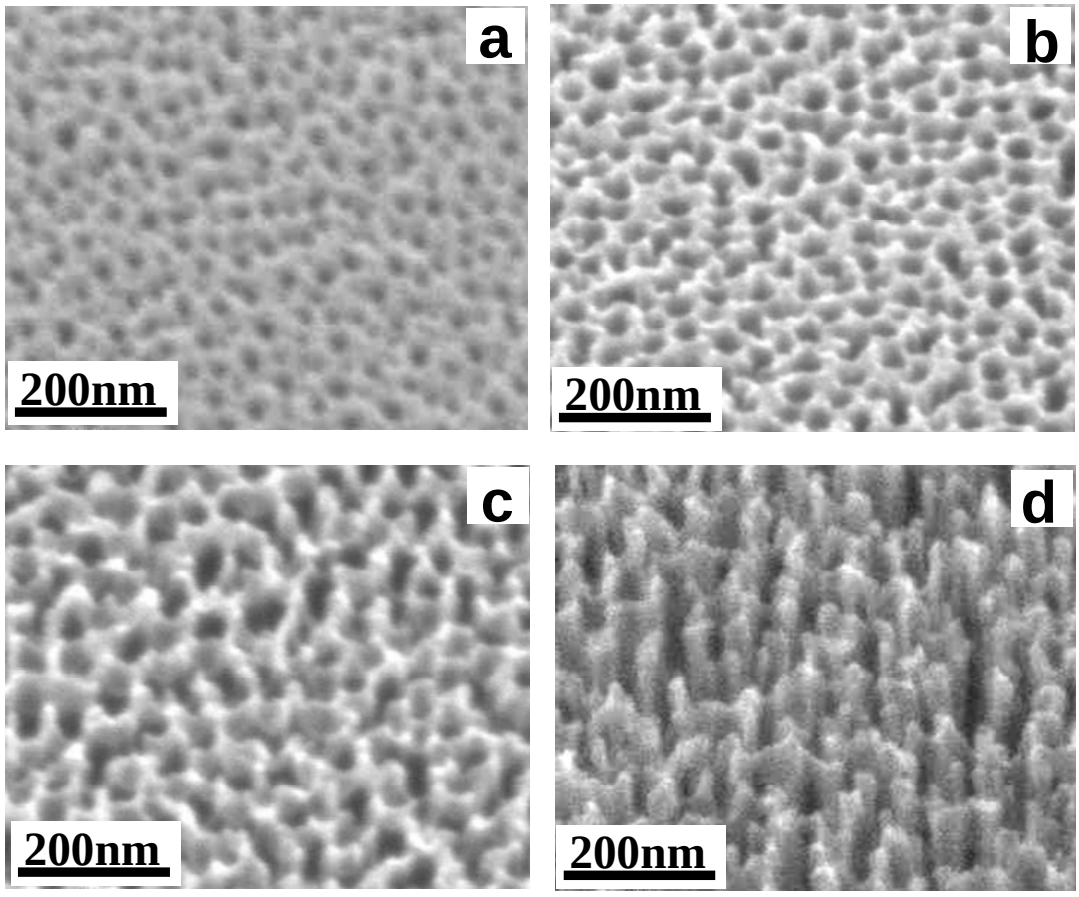

Figure 9. SEM images of AAO morphology etched in 0.51M phosphoric acid solution for etching different times. (a) 0 min, (b) 20min, (c) 40min, and (d) 55min. After ~55 minutes etching, a nanowire configuration begins to emerge.

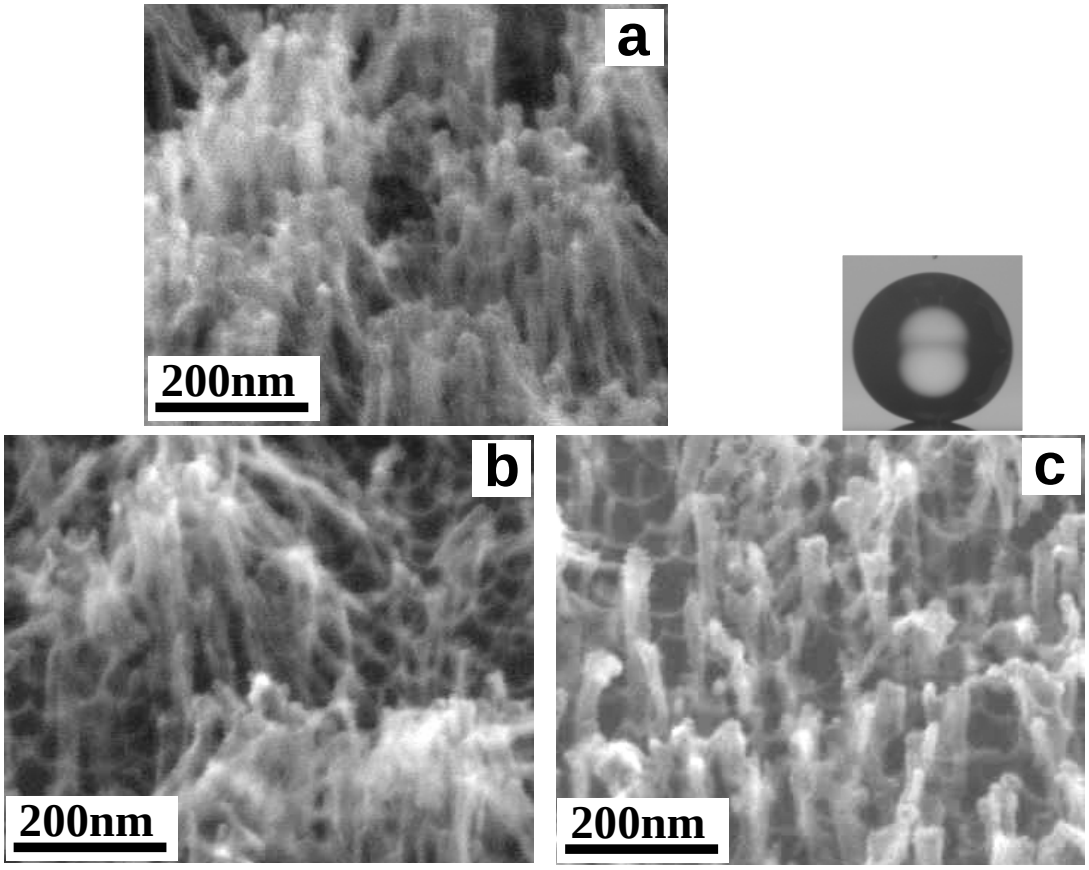

Figure 10. SEM images of fine Al_2O_3 nanowires made by pore widening or AAO nanopore samples. (a) after 65 min. etching, (b) after 70min. etching, and (c) 70min etching and supercritical CO_2 dried to minimize nanowire agglomeration. The wetting angle measurement (see water droplet in the inset) shows that the contact angle (CA) from this sample is quite large, ~169^o.

For AAO etching, NaOH solutions and chromic acid solutions have also been used and reported in the literature to fabricate alumina nanowires from aluminum.[32-34] However, fine Al_2O_3 nanowire formation on technically important non-aluminum substrate surface such as silicon or glass has not been investigated. Also, the hydrophobicity aspects of Al_2O_3 nanowires have not been studied yet.

For superhydrophobic surfaces, a coating is often required on the surface in order to reduce the surface energy. The simplest method is to use a thin layer coating of silanes with chloride or alkoxide groups. Trichloromethylsilane, trichlorosilane with fluorocarbon chains, and dimethylchlorosilane with fluorocarbon chains have been reported effective in reducing the surface energy.[37-39] However, chloride in the silanes produces HCl during polymerization with hydroxyl groups at the surface[40], and in our case this causes undesirable dissolution of alumina nanowires. Another water-repellent agent without chloride groups is (heptadecafuorodecyl-1,1,2,2-tetrahydrodecyl) trimethoxylsilane (FAS), which has been coated on the surfaces through vapor and solvent reactions.[41-43] The FAS coating was chosen as the coating material for our superhydrophobic nanowire surface. The hydrophobic coating of the Al_2O_3 nanowires was carried out in a methanol solution of hydrolyzed FAS at room temperature following the pore-widening chemical etching of the AAO.

The equilibrium contact angle (CA) of water droplet on a rough, highly hydrophobic surface can be calculated from the Wenzel model[1] for less hydrophobic cases and Cassie-Baxter model[2] for more hydrophobic cases. The Cassie-Baxter model is represented by the following expression:

$$\cos\theta_C = f(\cos\theta_S + 1) - 1 \tag{5}$$

where θ_C is the apparent CA, *f* is the projected area fraction of solid-liquid interface (nanowire area fraction in this case), and θ_S is the intrinsic CA of the droplet on a flat surface. As reported previously, the wettability of water on the AAO can be hydrophilic or hydrophobic depending on the geometry of AAO, the diameters of pores, and hole depths.[44] In this experiment, the CA of AAO with the hole diameter of 20nm and hole depth of 400nm prior to pore-widening etching (see Figure 9(a)) is measured to be 99^o, The CA of this AAO sample after FAS coating treatment becomes 129^o, which is likely in the Cassie-Baxter state.

Figure 11 shows the apparent CAs of water droplets on the AAO surfaces with FAS coating as a function of the pore widening etch time (The nanowire-structured surfaces, before the FAS coating, exhibit highly hydrophilic surface characteristics with very small contact angles below ~20^o.) As expected, the CA on the AAO increases as the etching time increases because the projected area fraction of solid-liquid interface (area fraction of protruding nanofeatures), *f*, in equation (5) is reduced, and also there is a transition from nanopore configuration to nanowire geometry. For an etching period in the range of 40 to 80min, relatively high values of CA (~150 – 170^o) are obtained. At an etching time of ~65-75min (see Figures 9(b) and (c) and on soda lime glass described later shown in Figure 11(c)), mostly nanowires are present, which produces an excellent superhydrophobic surface. However, on overetching of longer than ~80 minutes, the CA drops rapidly as the Al_2O_3 nanowires are beginning to erode away for eventual complete disappearance. The apparent CA of water on the Al_2O_3 nanowires can be calculated using equation (5). The intrinsic CA of a water droplet of a smooth surface of alumina after FAS coating is 117^o. The projected area fraction of solid-liquid interface

(protruding structure), *f*, is 0.89 for the initial AAO without etching, however, the value of f is reduced to 0.68 and 0.44 after etching for 30min and 45min, respectively, and *f* becomes progressively smaller with more etching time as expected. The anticipated CAs of water droplets for the etching times of 30min and 45min based on equation (5) are 132˚ and 142˚, respectively, but their measured values are 139˚ and 156˚. The red curve containing circled data points in the graph of Figure 11 represents the theoretical calculated CAs, which are approximately 10˚ below the experimentally measured CA values.

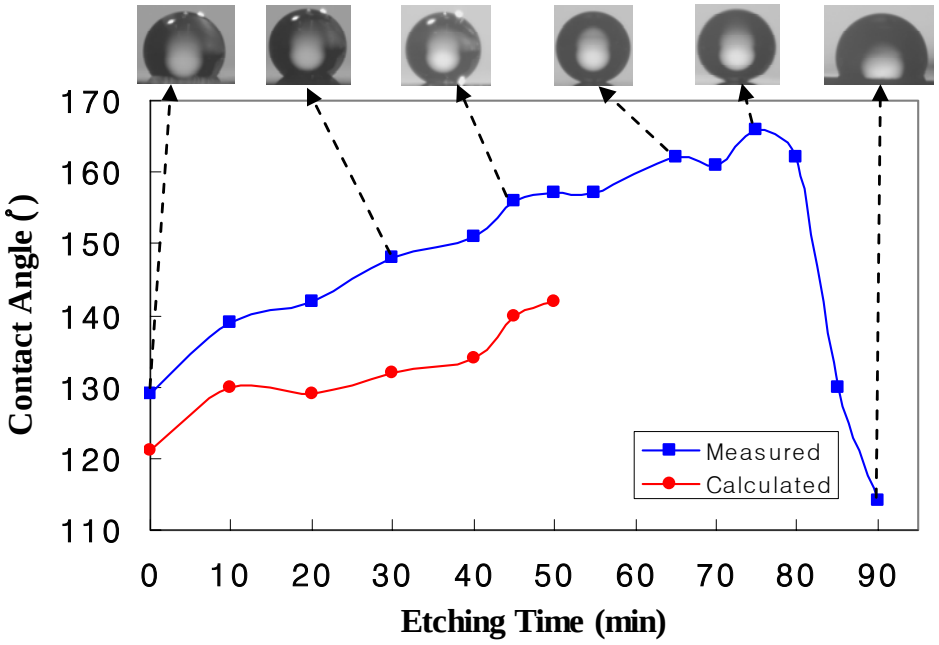

Figure 11. Contact angle of water on the FAS-coated AAO surface as a function of pore widening etching time. The lines are connecting the experimental data points. The nanopore regime is maintained up to the etch time of 0~50 minutes. The nanowire regime is produced for etch time of ~50 – 70 minutes, after which the nanowires are over etched and broken up into pieces.

In our calculations, the value of projected area fraction, *f*, was determined from a top view SEM picture of the etched porous alumina, and we assume that the top surface of the alumina sample is flat. However, the actual topography of the top surface of the porous alumina is not completely smooth with some height variations. In addition, the pore widening etch process, being isotropic chemical etching, tends to create a curvature and rounded nanowire tip or nanopore edge, which would give a larger projected area fraction than the actual contact area of the droplet with the top portion of the nanostructures. For these reasons, the real projected area fraction is probably less than the calculated values, with a consequence of the actual CAs being larger than the calculated CAs.

As can be seen from Figures 10(a) and (b), very fine and separated Al_2O_3 nanowires with smaller diameters (~10 – 40 nm diameter) tend to get agglomerated during drying from wet conditions, presumably due to the movement of liquid/air interface. In order to improve the microstructural configuration toward less agglomerated, vertically nanowire geometry, we introduced supercritical CO_2 drying, as shown for Figure 10(c). This produced more subdivided nanowires than the air dried sample for enhancing the superhydrophobic surface, with the resultant CA becoming larger and approaching ~169^o.

Having successfully obtained highly superhydrophobic Si surface decorated with Al_2O_3 nanowires, we then applied our alumina nanowire processing to a soda lime glass surface to create an optically transparent superhydrophobic glass. For application purposes, a non-wettable glass surface can be useful for self-cleaning windows. The transparency of porous anodic alumina films has previously been reported on glass

substrates, with the color of the substrate after anodization became a slight milky white color.[45] Figure 12 shows the optical images of a water droplet on a hydrophilic AAO porous layer (Figure 12(a)) vs. transparent superhydrophobic Al_2O_3 nanowires (Figure 12(b)) coated on the glass. The as-anodized AAO on the glass is hydrophilic with a CA of a water droplet of only 54^o. However, after etching for 65 min to produce a nanowire geometry and FAS coating, the sample surface becomes superhydrophobic with a large CA of 162^o. In this experiment, the color of the AAO on the glass is a slightly green color, but it becomes essentially perfectly transparent after 65 min etching and FAS coating as seen in Figure 12(b). The silver color around the edges of the glass sample is from the left-over original thin layer of deposited aluminum not subjected to the anodization process due to the insulating lacquer utilized during anodization.

Interestingly, it is noted that the shape of the Al_2O_3 nanowires fabricated on the glass substrate (~20 – 50 nm diameter) is different from that on the silicon substrate (Figure 10). The SEM image of the Al_2O_3 nanowires prepared on a glass substrate, Figure 12(c), indicates that the nanowires are better defined on the glass substrate as compared to those on a Si substrate (Figure 10(a)). All experimental fabrication conditions for Figure 10(a) and Figure 12(c) are identical except for the substrate material. The exact reason for such a difference in nanowire geometry with the choice of substrate material is not clear, however, it may be caused by that fact that AAO on silicon substrate is hydrophobic while AAO on glass substrate is hydrophilic as evidenced by contact angle measurements. During the pore-widening etching, the bottom part of the pores with a hydrophilic surface can be reached easily by the

phosphoric acid etching solution, and the chemical etching near the bottom portion of the pore can be easier and more uniform for the case of AAO on a glass substrate. By contrast, air pockets are often trapped underneath the solution in the case of hydrophobic substrates,[32, 44] which may lead to uneven etching of the pores. The contact angle for the sample of Figure 12(c) is ~162^{o}.

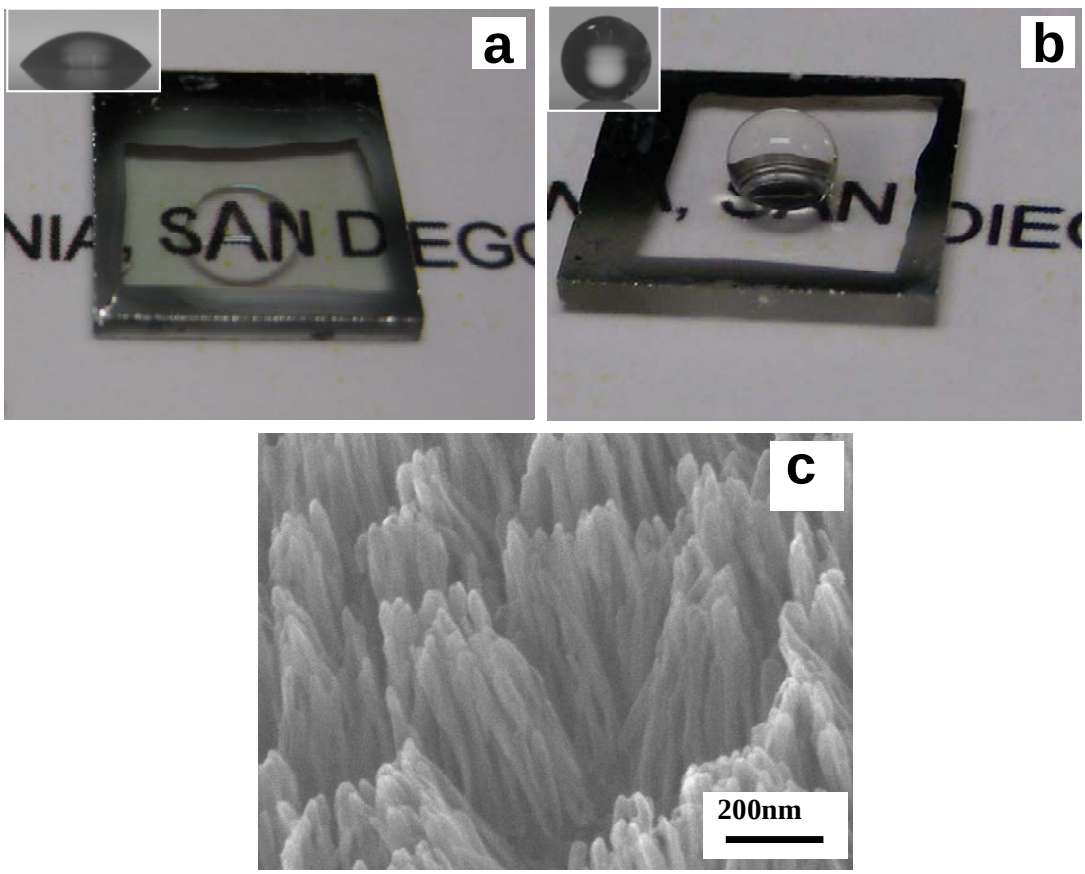

Figure 12. The images of water droplet on AAO coating on soda lime glass. (a) with as-made AAO on soda lime glass (CA = 54^{o}), (b) Al_2O_3 nanowires on soda lime glass after 65 min pore-widening etch and FAS coating (CA = 162^{o}), and (c) SEM image of Al_2O_3 nanowires in Figure 11(b). The insets show water droplet contact images on measuring the contact angles.

The optical properties of the glass coated with superhydrophobic Al_2O_3 nanowires was also evaluated. Figure 13 shows the spectrophotometer measurements data for the glass with Al_2O_3 nanowires vs. a bare glass slide (used here as a reference control sample). Light transmittance through the glass with Al_2O_3 nanowires was measured in both directions, through the top and bottom. The value of light transmittance through the top (light incident onto the top surface of the Al_2O_3 nanowires) is slightly higher than that through the bottom (light incident from the bottom surface of theAl_2O_3 nanowires) when the wavelength is greater than ~350nm.

Figure 13 also shows that the light transmittance of the alumina nanowires through the top surface is slightly less than that for the glass slide within the UV spectra regions of 300 - 520nm. Such a reduced UV transmission is desirable for some glass window applications. In the visible spectra regions beyond ~500 nm, we observed a slightly more light transmission in the nanostructured glass than that for the bare glass, which might be caused by the antireflection effect of alumina nanowires,[22] especially for the 540-800nm regime.

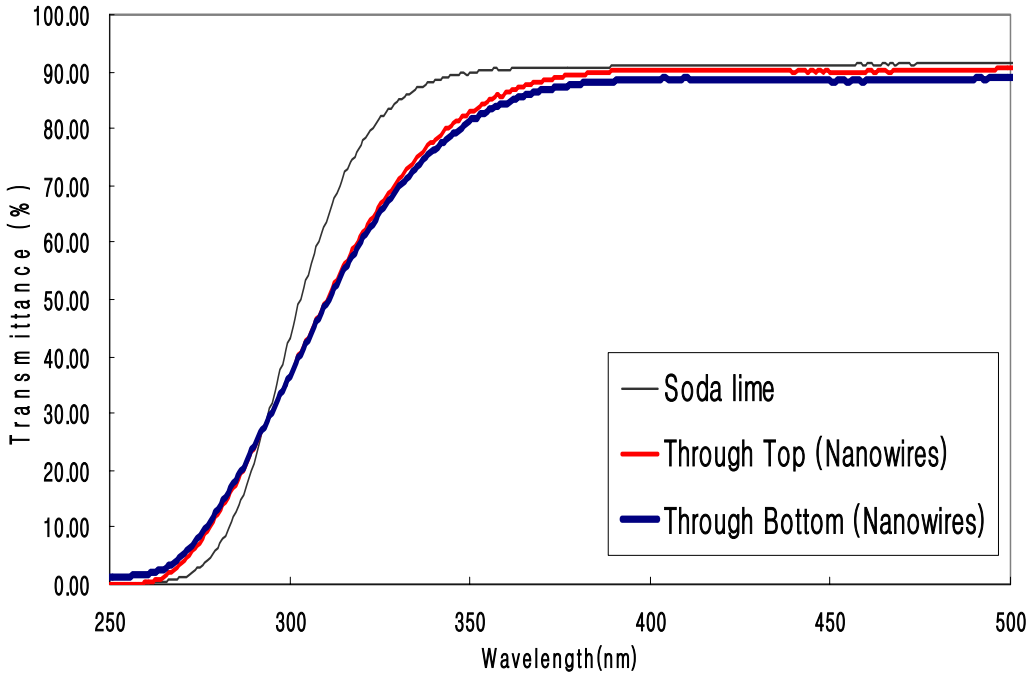

Figure 13. Spectrophotometer measurement of the superhydrophobic surface of alumina nanowires coated on soda lime glass (Figure 11(b)). The light was penetrated through the top (alumina nanowires) and bottom (glass substrate), respectively. The optical transmission of the untreated glass was also measured for comparison.

2.4 Summary

In summary, an Al_2O_3 nanowire topography on a substrate in a vertically aligned configuration was fabricated by altering the geometry of as fabricated anodized aluminum oxide pore structures through pore-widening chemical etching. Optimized etching and supercritical CO_2 drying produced very fine ~20 –40 nm diameter Al_2O_3 nanowires which exhibit superhydrophobic characteristics, with a very high water droplet contact angle as high as ~169^o. Optically transparent yet highly superhydrophobic glass can be prepared by introducing the aligned Al_2O_3 nanowire structure on the glass surface. Optical property evaluations indicate that such a nanowire-decorated glass substrate exhibits slightly less light transmittance in the UV regions but more transmittance in the visible spectrum region than the bare untreated glass. Such a ceramic surface nanowire can be useful for creating self-cleaning, durable and superhydrophobic surfaces on a variety of materials especially window glass type materials. The water repellent glass can potentially be utilized as an environmentally friendly material to save water for cleaning and reduce the usage of chemicals for cleaning of windows, buildings and various other structures.

This chapter, in full, has been published as “Optically Transparent Glass with Vertically Aligned Surface Al_2O_3 Nanowires Having Superhydrophobic Characteristics”, by J.-Y. Kim, K. Noh, C. Choi, K. S. Brammer, M. Loya, L.-H. Chen and S. Jin, *NANO* (Vol. 4, No. 2, 2010, in press).

CHAPTER 3: Superhydrophobic Glass with Engineered Surface Nanostructures and Optical Properties

In this research a simple, cost-effective method was used to fabricate superhydrophobic glass surfaces with an extremely high water droplet contact angle. We have achieved a contact angle as high as 172 ^{o} by the straightforward and economical techniques of dry and wet etching methods in the aid of particle-like Ag etch mask to form nanopillar configurations for enhanced hydrophobic surface properties. Such a nanopillar decorated glass substrate would be of great interest to satisfy industrial needs by creating water-repellent glass with low cost methods. In addition to an induced superhydrophobic surface layer, an optically transparent surface comparable to untreated glass was achieved in the dry etched glass condition while a translucent property was obtained in the wet etched glass condition. The variation in optical properties can be unique to applications in both clear and tinted glass types.

3.1 Introduction

Clean technology, which is also called environmental or green technology, is an important field for sustainability of human races on earth. Water is often used for washing and cleaning of automobiles, house windows and high-rise building windows. Self-cleaning have been advancing in recent years. Potential applications of self-cleaning coating range from window glass, building exterior, textiles for reducing the usage of water, cleaning chemicals and labor costs, to processes and materials for enhancing safety and reliability in transportations and communications by minimizing dirt or snow accumulations on airplane windows, wing and telecommunication antennas.

Ag nanoparticles are often used in the fabrication of silicon nanowire arrays on silicon substrates using the electroless etching (EE) approach[46-49] as well as making superhydrophobic surfaces with high reflectivity.[50] Simple methods have been utilized for fabrication of superhydrophobic glass using Ag nanoparticles and the etching processes. A glass substrate decorated with nanopillars was created by both dry and wet etching methods, which exhibits optically transparent and translucent properties, respectively.

3.2. Experimental details

3.2.1 Materials and superhydrophobic glass fabrication

Glass microscope slides (Fisher Scientific, Fisherfinest) were used as substrates for the experiments. For fabrication of Ag islands on the substrate, Ag film was evaporated on the glass substrate using E-beam evaporator (Temescal BJD 1800). The annealing of Ag film with 5nm to 40nm thickness was done at the temperature range of 300℃ to 550℃ in a furnace with programmable temperature controller (Applied Test System, Inc.). Reactive ion etching (RIE, Oxford Plasmalab 100) was used to make pillar shaped arrays on glass surface using Ag islands as an etching mask for the dry etching. 0.5wt. % hydrofluoric acid (HF) solution was used for the chemical etching to control pillar shape with different etching times.

The creation of superhydrophobic glass surface was initiated using the metal ball-up process for the deposited metal layer first, followed by the etching step. As illustrated in Figure 14, Ag thin film was first deposited on the surface of glass and annealed at various temperature in order to break the as-deposited continuous Ag film

into particle-like Ag islands, which will serve as an etch mask hereafter. Reactive ion etching (RIE) was utilized to create nanopillar arrays. In case of wet etching process ((a), (b), (e), (f), and (g) in Figure 14), Au film was carefully vacuum deposited over the balled-up Ag islands to serve as a protective layer but not to cover the sidewall regions where the Ag island and glass substrate contact each other. This was carried out so that the chemical etchant is directed to etch through these specific sidewall regions in order to form nanopillar arrays.

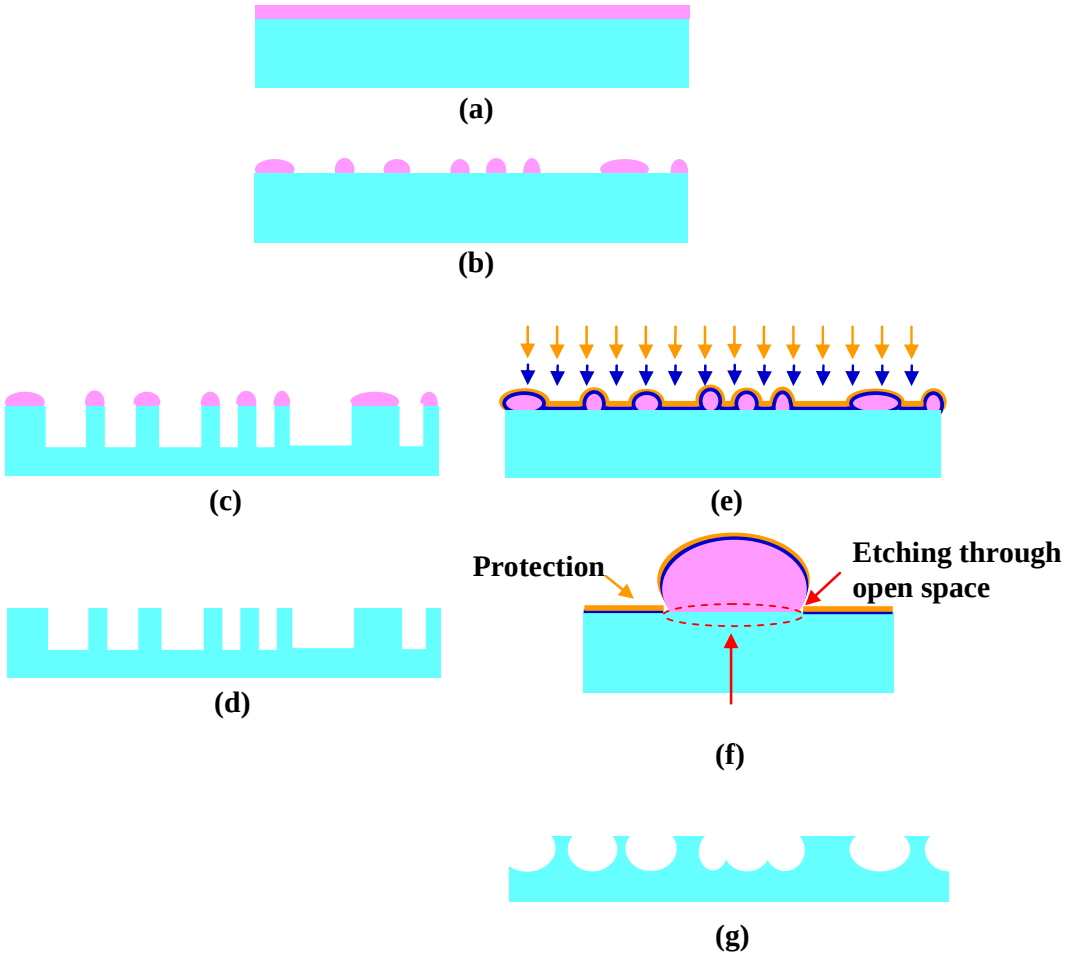

Figure 14. A schematic diagram of superhydrophobic glass fabrication. (a) Ag coating on glass, (b) balled-up Ag islands, (c) RIE using Ag mask for nanopillar formation, (d) optional removal of Ag island mask to expose vertical nanopillar array, (e) Ti+Au deposition as a protective layer, (f) magnification of (e); chemical etching through exposed shadow region (open space) with no Ti/Au coating. Ag islands also help to increase glass etching, and (g) remove Ag and Ti/Au layer.

3.3.2 Hydrophobic coating and sample characterization

The nano/microstructure of the processed glass specimen surface was examined by using a field emission scanning electron microscope (FE-SEM: Phillips, XL30 ESEM). Since the sample is glass, electron charge accumulation effect and associated image blurring was noted. Therefore, the sample surface was metalized for enhanced SEM imaging analysis. The optical transmittance of the sample was measured with a spectrophotometer (Varian Inc., Cary 500). Water droplet contact angles of the samples were measured with the sessile drop method with Video Contact Angle System (AST product Inc., VCA 2500XE and KSV Instruments Ltd., CAM100) containing analysis software. Instead of a macro-pipette, we prepared and used a micropipette/needle with less surface area in order to facilitate the measurement of contact angles. Such a micropipette was fabricated from a quartz capillary tube (1.0 mm outside diameter and 0.7 mm inside diameter) by using a pipette maker (Sutter Instrument Co., P-2000), followed by a hydrophobic coating of the micropipette surface, which allowed an easy transfer of the droplet to the sample surface. Also, the sliding angles were measured instead of the receding angle and the advancing angle because of difficult measurement of these angles due to high water droplet contact angles of the samples.

For superhydrophobic surfaces, a hydrophobic coating is often required on the surface in order to reduce the surface energy, especially for surfaces having hydrophilic nature such as glass. One method is to use a fluoroalkylsilane (FAS) as a hydrophobic coating, which has been coated on the surfaces through vapor or solvent reactions.[41-43] Hydrophobic surface coating on the nanopillar structured glass surface for enhanced superhydrophobicity was achieved by coating of (heptadecafurodecyl-1,1,2,2-

tetrahydrodecyl) trimethoxylsilane (FAS) (with a formula of $CF_3(CF_2)_7CH_2CH_2Si(OCH_3)_3$, produced from Gelest, Inc., No. SIH5841.5). The 1 wt % FAS solution was prepared in methanol solution. Next, the hydrophobic coating was carried out at room temperature following the process of surface nanopillar formation made by both dry and wet etching process and after Ag island removal for enhanced transparency. Samples were immersed into the FAS solution at room temperature for 2 h, and subsequently dried in the oven at 130℃ for 1h.

3.3 Results and Discussion

3.3.1 Dry etching method

Ag films (2nm, 5nm, 10nm, and 15nm) on glass surfaces were deposited by the evaporation process, followed by annealing treatment in a quartz furnace (Applied Test System, Inc.) under vacuum condition for 1hr at temperatures of 300, 400, and 500℃ which are below the glass transition temperature (around 630℃) of the soda lime glass used. Annealing temperature did not affect the diameter of Ag islands significantly. The average Ag island diameter was 5nm, 10nm and 15nm Ag film after heat treatment of 20nm, 45nm and 90nm, respectively. A silver film thickness of 2 nm was found to be too thin as the Ag balled up islands were rather ununiform in size and shape. Figure 15 to 18 shows the morphologies of different Ag films at the different sintering temperatures. As seen in Figure 15 to 18, the surfaces of deposited Ag films are very rough because Ag is one of the novel metals, causing week adhesion to the most

surfaces and inducing non-smooth surface. On heating, Ag films are easily broken up and changed to island geometry by relatively low temperature annealing.

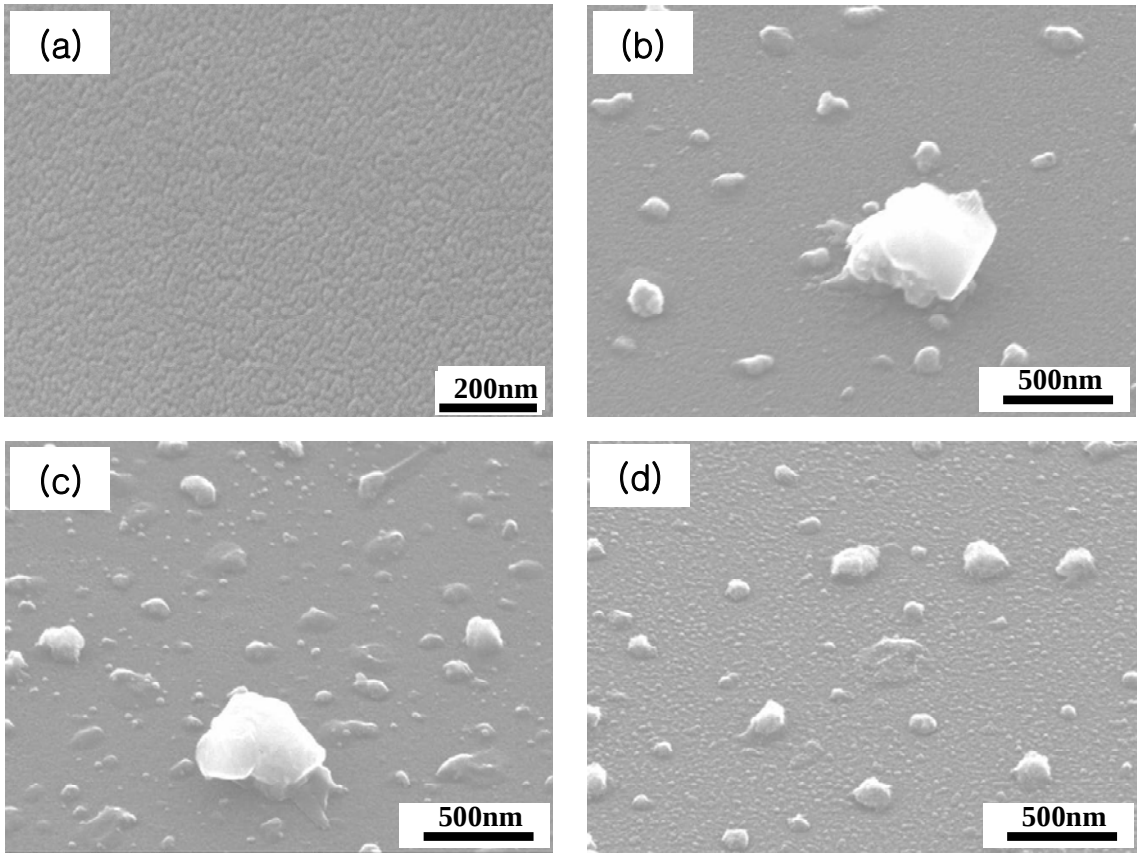

Figure 15. SEM images of 2nm Ag film at various sintering temperatures. (a) as-coated, (b) 300℃, (c) 400℃, and (d) 500℃ annealing temperature.

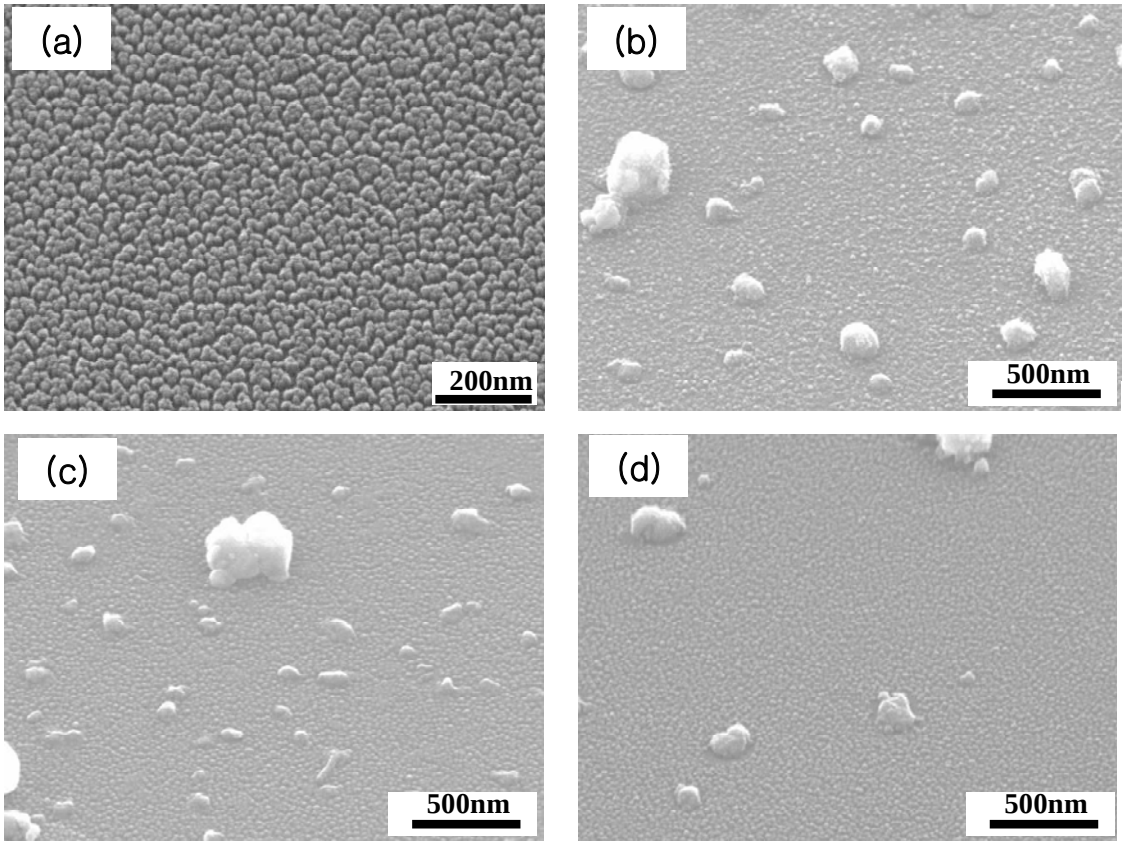

Figure 16. SEM images of 5nm Ag film at various sintering temperatures. (a) as-coated, (b) 300℃, (c) 400℃, and (d) 500℃ annealing temperature.

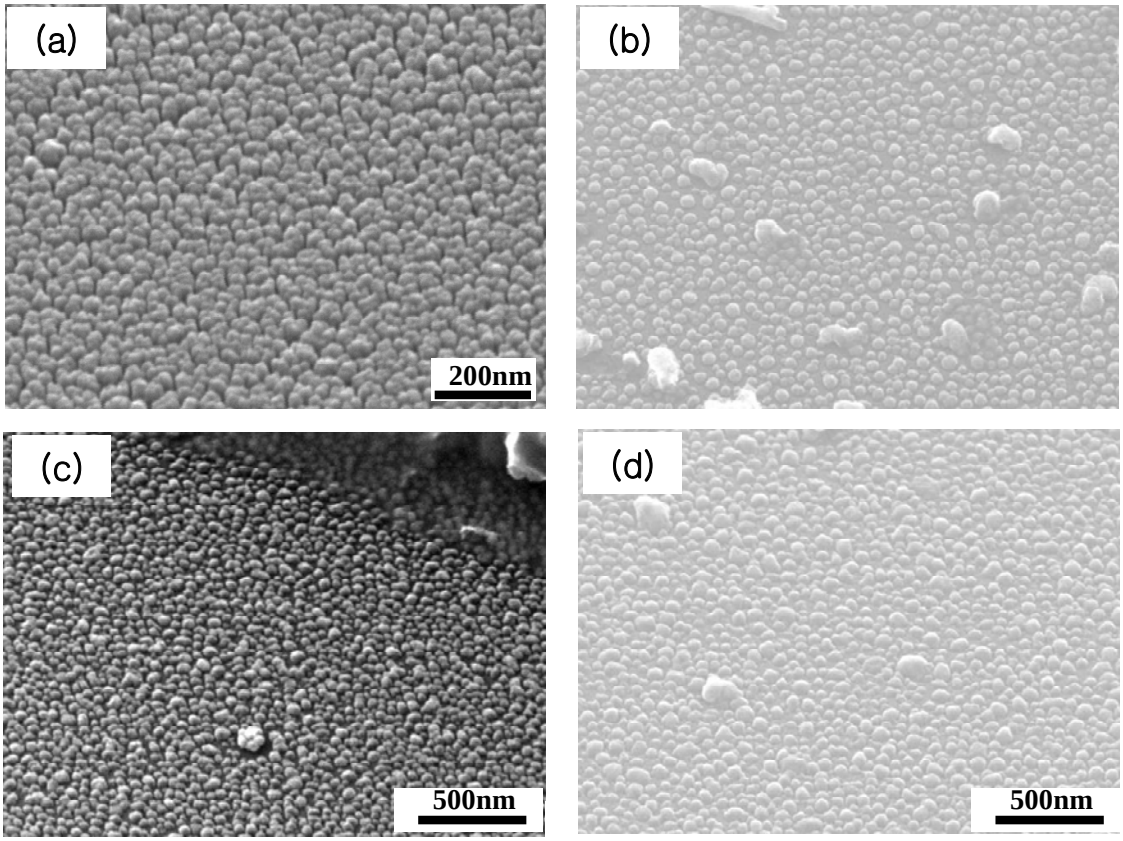

Figure 17. SEM images of 10nm Ag film at various sintering temperatures. (a) as-coated, (b) 300℃, (c) 400℃, and (d) 500℃ annealing temperature.

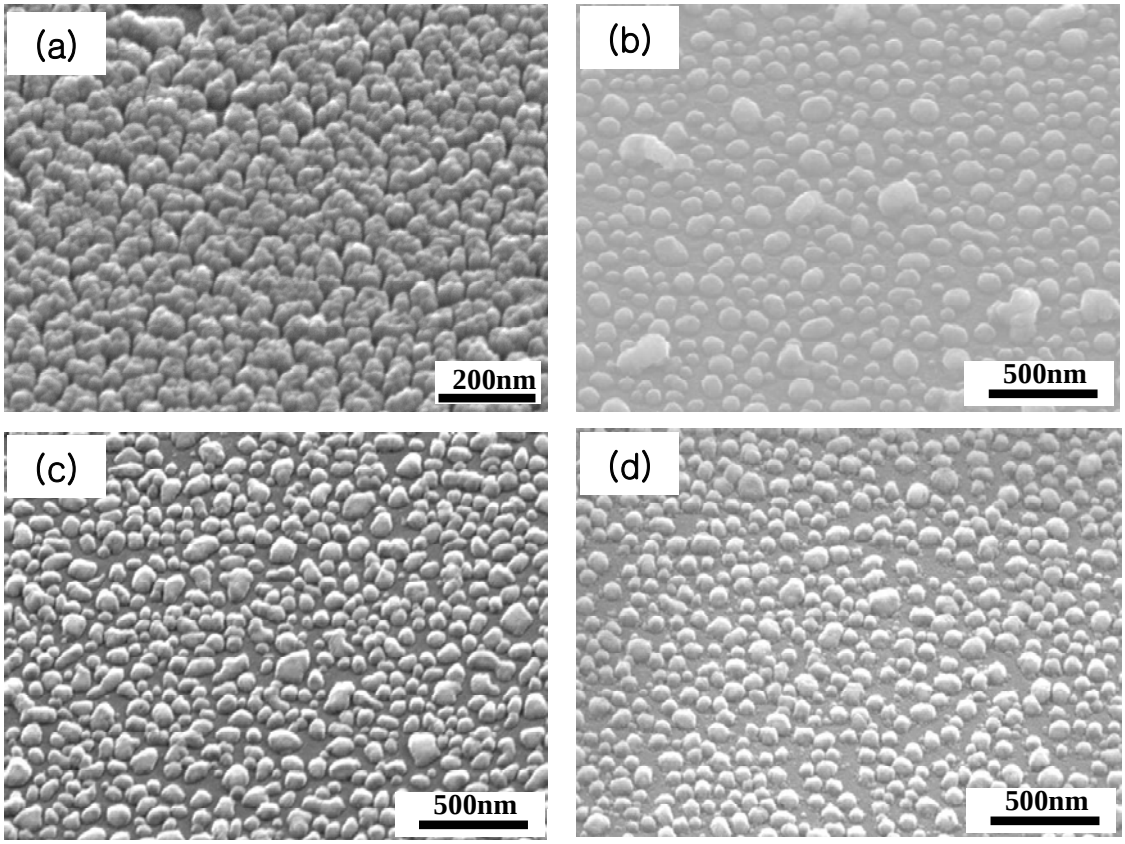

Figure 18. SEM images of 15nm Ag film at various sintering temperatures. (a) as-coated, (b) 300℃, (c) 400℃, and (d) 500℃ annealing temperature.

Figure 19 shows the measured CA of a water droplet on the nanoopillar arrayed glass samples as illustrated in Figure 14a-14d for the dry etching conditions. Figure 19a shows a field emission scanning electron microscope (FE-SEM: Phillips, XL30 ESEM) image of Ag islands used as an etch mask formed from a 15nm thick Ag film annealed at 500℃. As shown in Figure 19b, the nanopillar structure is well developed, simply formed by RIE and successive Ag island removal. A trend is revealed that the CA of a water droplet increases from 110˚ to 170˚ as initial Ag film thickness also increases.

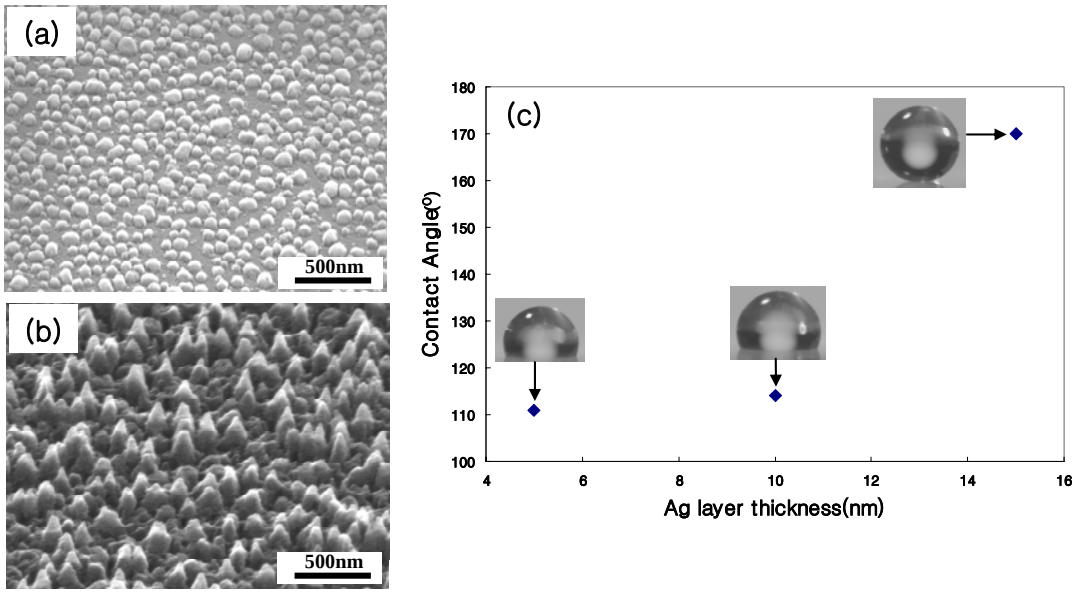

Figure 19. SEM images and CA of a water droplet of Ag ball-up and RIE process. (a) SEM image of 15nm Ag film on glass substrate after annealing at 500℃, (b) nanopillar formation on the glass surface made by RIE process, and (c) contact angle of water droplet vs. deposited Ag layer thickness for RIE etched glass.

3.3.2 Wet etching method

In regards to wet etching approach to make a superhydrophobic surface, we increased the Ag film thickness up to 40nm and conducted similar process as mentioned before. Figure 20a shows Ag islands after annealing at 550℃, with nominal diameter is ~150 nm. For the wet etching procedure, heat treated glass with Ag islands is dipped into 5 wt % hydrofluoric acid (HF) in DI water solution for 20 seconds as shown in Figure 20b. At the very beginning of the etching process, the regions located nearby the Ag particles are etched faster than those exposed directly to etching solution, leaving crater-like etch pits underneath the areas where Ag islands are in direct contact with the glass. This might be due to a catalytic type etching occurring at the surface,[46-48] even though no oxidizing agents such as H_2O_2 and $Fe(NO_3)_3$ were present under our etching conditions. It has been shown, however, that the processing of etching is significantly enhanced under situations where silicon wafers are immersed into mixed $AgNO_3$ and HF solution with H_2O_2.[49] In addition, glass is readily etched in the HF based solution so that extended etching eventually nullifies the preferential etching effect seen at the beginning stages of etching.

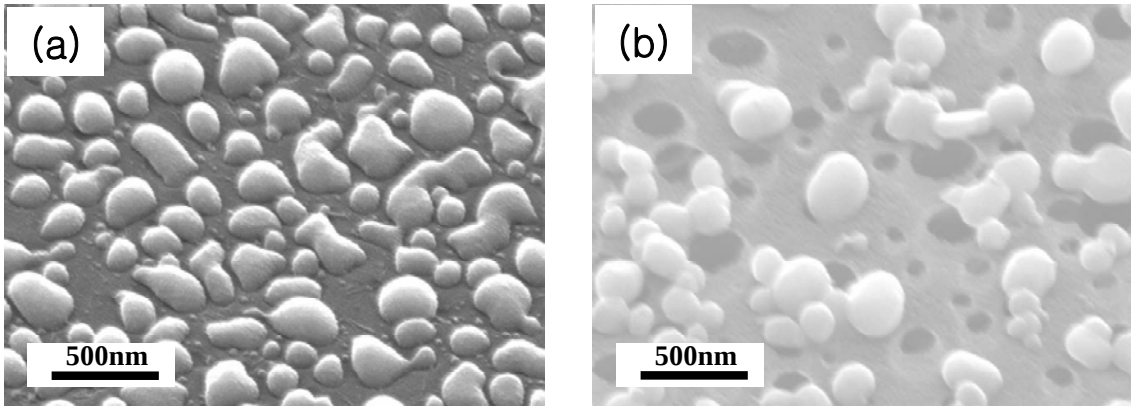

Figure 20. SEM images of 40 nm Ag ball-up and subsequent chemical etching. (a) Ag islands of 40 nm film thickness after heat treatment for 1hr at 550℃, and (b) the surface morphology of glass after chemical etching in 5wt % HF solution for 20 seconds.

Next, 5 nm Ti and 20 nm Au was deposited as a protective layer to prevent the exposed surface of the glass from dissolving in HF solution. Because the Ag islands have a spherical curvature, areas around the Ag islands on the glass surface are left uncovered from the Ti+Au protective layer, as seen in Figure 14f. HF solution can penetrate through these shadow regions and preferentially etches the glass. Figure 21 shows the morphology of glass surface etched in 5wt% HF solution for different etch times. The main advantages of this etching approach is (i) the simplicity, (ii) ease of fabrication, and (iii) the overall low cost method used to create nano and micro scale patterns for making superhydrophobic surface properties on glass by using an HF based solution, which is a well known isotropic etchant.

At short etching times, holes are created underneath Ag islands in Figure 21(a). As shown in Figure 21(b), the size and density of holes increase with increasing etching time. With even more etching time, the structure of the glass surface represents a thin and discrete roof shape top supported by the pillars formed after 40 second of etching (Figure 21©), which can be further distinguished by Figure 21(d) after 43 second etching. Eventually, there are nano-sized pillars with traces of thin roofs on the tips. Upon further etching, for up to 48 seconds, results show a pillar formation with another type of thin rough structure on the top (Figure 21(e)). The glass pillars are completely etched away with an etching time over 55 seconds, resulting in just a trace of the pillars (Figure 21(f)).

Similar to the dry etching procedure, FAS coating was performed after wet etching at the various etch times and Figure 18 shows the apparent CAs of water droplets on the glass surfaces as a function of the etching time in dilute HF solution. As

expected from Figure 21, the CA on the glass surface increases as the etching time increases because, as described previously, the projected area fraction of the solid-liquid interface in Cassie-Baxter equation is reduced. The CA increases from 110^{o} to 172^{o} when the chemical etching is increased from 20 second to 48 second. CAs exceeding 150^{o} were obtained during the etching period in the range of 43 to 52 seconds, and the highest CA achieved peaked at 172^{o} after 48 second of etching. Although the trend in Figure 22 illustrated that CA increased with increasing etching time, the CAs started to decrease after an etching time of 48 seconds and beyond, probably because the pillars on the glass surface were beginning to disappear. After 70 seconds of etching time, most the pillars have been completely etched away and the CA showed only 114°. In terms of water repulsion and superhydrophobicity, the low contact angle hysteresis and sliding angle are also important regarding the mobility of a water droplet.[37, 51, 52] To further characterize our superhydrophobic surfaces, we measured the sliding angles. The sliding angles fabricated by RIE (Figure 19(b)) and chemical etching (Figure 21(e)) are 7^{o} and 10^{o}, respectively. The RIE method shows a slightly lower sliding angle, and we believe this is due to differences in the nanopillar structures, particularly the nanopillar sharp tip shape.

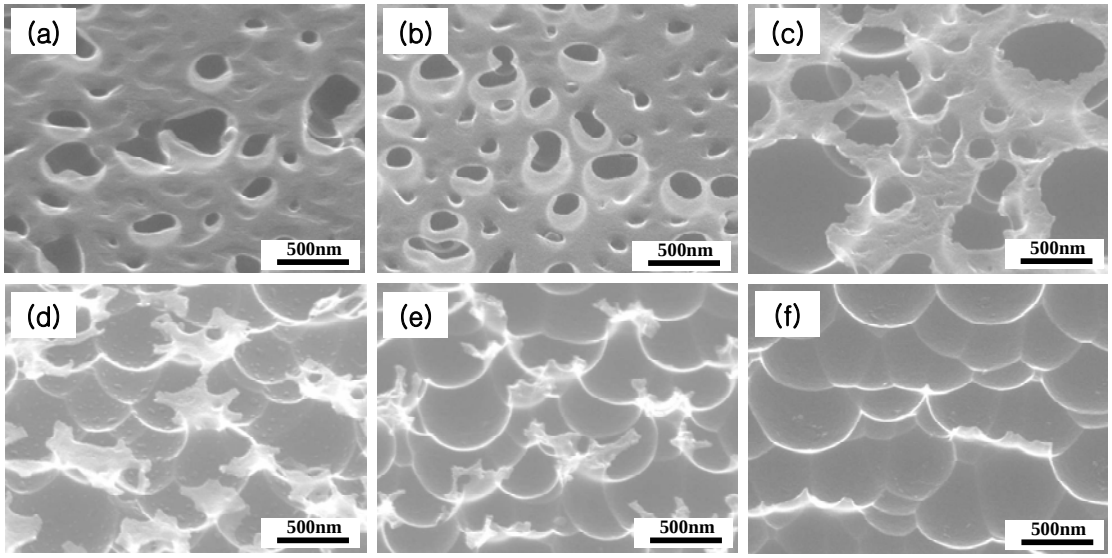

Figure 21. SEM images of morphology of glass surface in 5wt% HF solution for etching different times after Ag ball-up and metals (Au/Ti) deposition. (a) 20, (b) 30, (c) 40, (d) 43, (e) 48, and (f) 55 seconds.

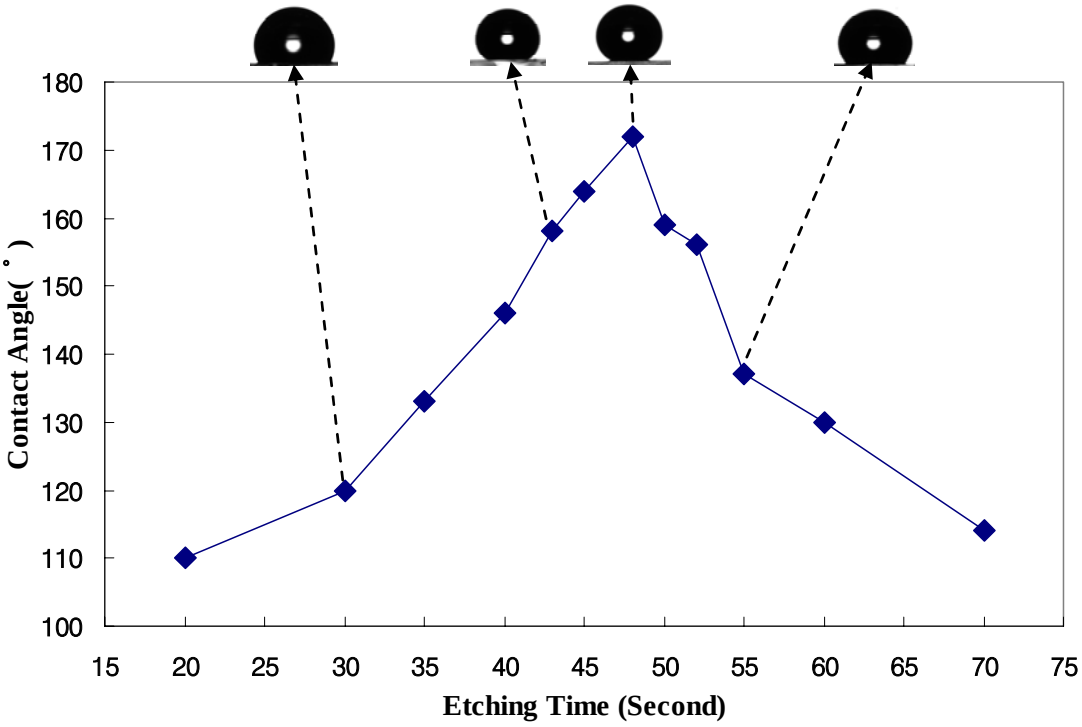

Figure 22. The contact angles of water drop on the FAS-coated glass surface as a function of etching time in 5wt% HF solution.

3.3.3 Optical property

We have also evaluated the optical properties of the glass with nanopillars on the surface using a spectrophotometer (Varian Inc., Cary 500). Figure 23 shows the spectrophotometer measurement and the image of water droplet (inset) for nanopillars having Ag islands on the top of the pillars (refer to Figure 19(b) with Ag islands on the top of pillar). As shown in Figure 23, the glass with the Ag island mask (not yet removed) has a non-symmetrical light transmission, where the light transmission from one side of the glass in very different from the light transmission through the opposite direction, illustrating what appears to be a one-way mode of transmission. Its contact angle (CA) is 158^{o}, which is a little lower than the CA of glass after removing the Ag islands. The light transmission from the bottom to the top shows slightly suppressed transmission in the UV to visible wavelength regime of about 320 to 800 nm, while the light transmission from the top to the bottom is highly asymmetrical with particularly suppressed transmission in the UV to violet wavelength range of about 330 to 450 nm. Such an asymmetrical glass can be utilized for special window applications needing this specific optical property.

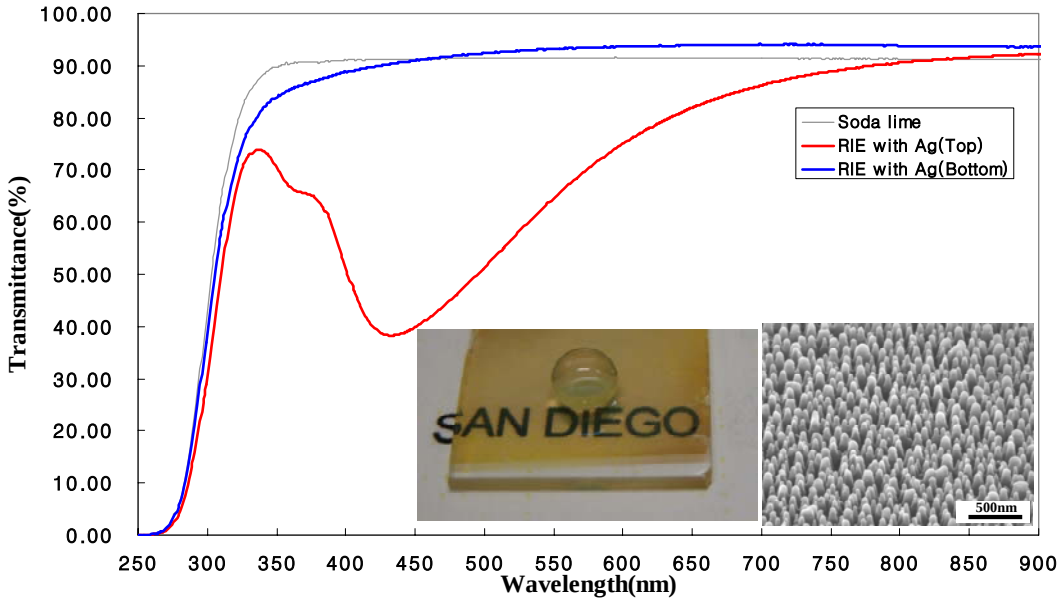

Figure 23. Spectrophotometer measurement demonstrating a non-symmetrical optical transmission through glass with leftover Ag islands made by RIE etching. The insets show an image of a water droplet and SEM image of the nanopillar structure on glass with Ag islands on the top.

Figure 24 (a-c) represents the optical properties and images of nanopillar glass surfaces shown in Figure 19(b) (dry etching) vs. Figure 21(e) (wet etching), respectively. Interestingly, the two surfaces uniquely represent UV-reducing (sample of Figure 19(b)) and tinting (sample of Figure 21(e)) optical transmission properties. Superhydrophobic glass made by Ag ball-up and RIE etching shows UV low transmittance (320 ~ 450nm) and the same or slightly better transmittance in the visible wavelength (450~750nm) than bare glass, which may be due to the antireflection effect of nanopillars.[22] In contrast, superhydrophobic glass fabricated by wet chemical etching shows translucent property like a tinted glass, which is most likely due to the larger size of the nanopillars and possibly the non-uniform morphology compared to structure made by dry RIE etching. Figure 24(b) and 24(c) show the representative images of a water droplet on the glass surfaces made by RIE and chemical etching, respectively. In the figure 24(c), the left half (translucent) of the image is superhydrophobic glass made by wet chemical etching, and the right half (transparent) is the untreated, control soda lime glass sample.

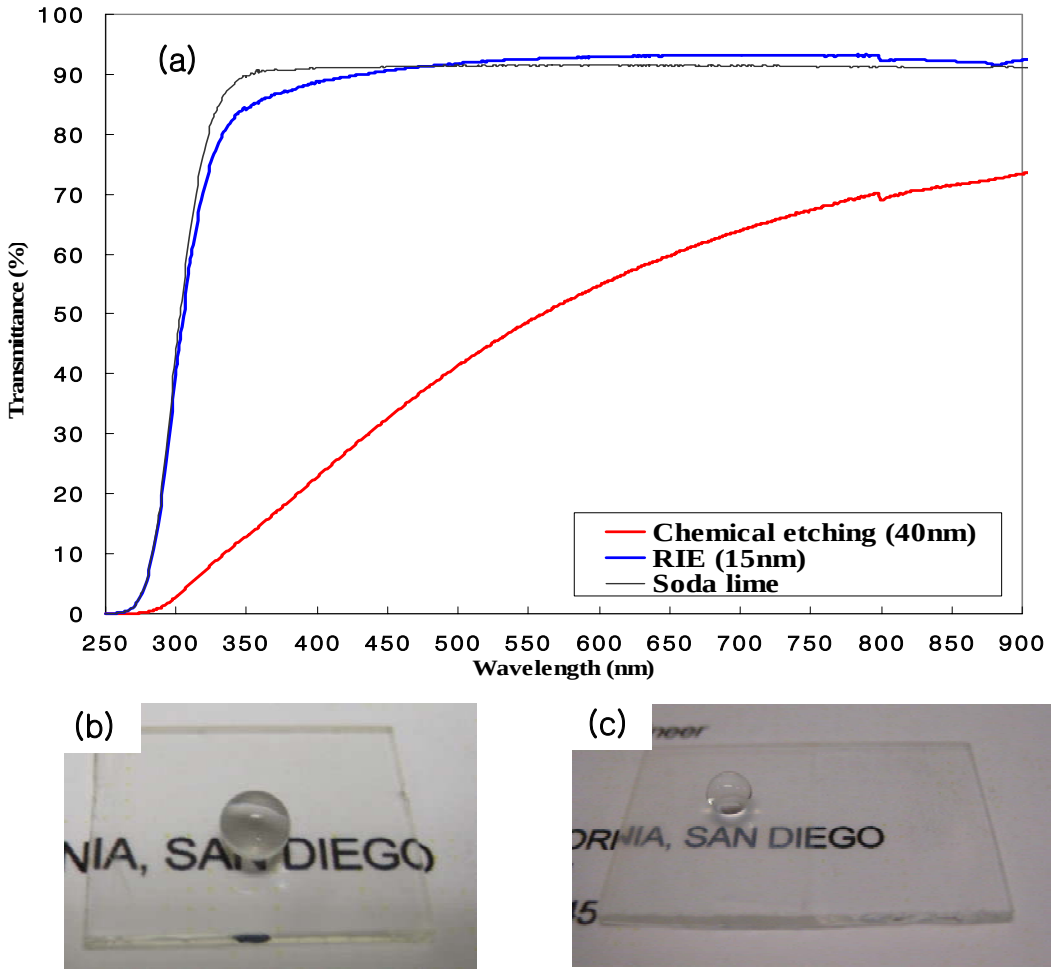

Figure 24. Spectrophotometer measurement and images of water droplet on the surface of glass made by RIE and chemical etching. (a) Spectrophotometer measurement of RIE (Figure 19(b)) and chemical etching (Figure 21(e)), (b) the image of water droplet of glass made by RIE, and (c) the image of water droplet of glass made by chemical etching.

3.4 Summary

Superhydrophobic glass with an extremely high water droplet contact angle (CA) as high as 172 ^{o} has been successfully fabricated by the simple methods comprising of Ag deposition, heat treatment, and RIE/chemical etching processes. These methods can be applied to large areas of glass, which is of significant importance for industrial applications such as building windows and display screens. It has also been demonstrated that optically transparent or translucent superhydrophobic glass can be prepared by the different etching methods utilized. In the case of dry etching, nanopillar decorated glass surfaces are created, which exhibit slightly less light transmittance in the UV regions but more transmittance in the visible spectrum region than bare untreated soda lime glass. Glass substrates fabricated by the chemical etching route give a translucent optical property. Both etching techniques give rise to unique superhydrophobic and optical properties. Such a glass with nanopillars on the surface can be useful for creating self-cleaning characteristics on a variety of materials especially window glass type materials. Additionally, the nanopillars themselves are made directly from the glass substrate by surface removal of materials rather than deposition of foreign materials, which means the structure is very durable and robust.

This chapter, in full, has been prepared for “Fabrication of Optically Transparent and Translucent Glass Having Superhydrophobic Characteristics”, (In preparation) by J.-Y. Kim, C. Choi, K. Noh, K. S. Brammer, L -H. Chen, and S. Jin. The dissertation

author was the primary investigator and author of this manuscript being prepared for submission for publication.

CHAPTER 4: Superhydrophobic Glass Coated with Teflon Nanopillar Arrays Created from Diblock Copolymer Thin Films

The technical approach used for this research employs the self-assembled structure of block copolymer as nanometer etching masks. Teflon nanopillar arrays were fabricated with gold nanoparticles made from polystyrene-*block*-poly (4-vinylpyridine) (PS-*b*-P4VP) diblock copolymer as etching masks. It was found that the cylindrical microdomains of PS-*b*-P4VP can not be formed directly on Teflon coating itself. This problem can be solved by introducing oxygen plasma to activate the surface of Teflon and improve wettability of Teflon surface relative to the solvent (Toluene/THF) which contains PS-*b*-P4VP. Gold nanoparticles introduced and embedded into P4VP blocks (because of the hydrophilic nature of P4VP blocks with affinity to Au-containing solution) were utilized in this research as etching masks to fabricate Teflon nanopillar arrays. Teflon nanopillar-decorated glass substrate exhibits a very large water droplet contact angle as high as 168^{o}, while an excellent optical transparency is still maintained.

4.1 Introduction

The self-assembly of block copolymers leads to unique structures in which the repeated units exist only in long sequences of the same type, and well-ordered morphologies such as spheres, cylinders, and lamellae depending upon the volume fractions of the blocks.[53] It is well known that the block copolymers can have extremely dense and well-ordered periodic nanostructures. Diblock copolymers are

considered to be attractive candidates as templates and scaffolds for nanostructure and inorganic nanodot fabrication over large area.[54-60] To achieve the desired long range ordering and hexagonally close-packed vertical cylindrical morphology, approaches such as balancing interfacial interaction, electric fields, and chemically patterned substrates have been successfully applied.[61-63] Fluorinated polymers including polyterafuoromethylene (PTFE), commonly known as Teflon, have been used to fabricate superhydrophobic surfaces.[64-67] Unlike insoluble PTFE in organic solvents due to its semicrystalline property, Teflon AF (Dupont) is an amorphous polymer which increases its solubility, making it useful for coating on the surfaces.[68-70]

In this research, Teflon AF and polystyrene-*block*-poly (4-vinylpyridine) (PS-*b*-P4VP) coatings on a glass substrate were used to fabricate superhydrophobic surfaces. Teflon nanopillar arrays were fabricated using somewhat periodic Au nanoparticles synthesized from PS-*b*-P4VP as etching masks.

4.2 Experiment Procedure

4.2.1 Materials and Fabrication

Glass microscope slides (Fisher Scientific, Fisherfinest) were used as substrates for this experiment. Piranha solution, a mixture of sulfuric acid (H_2SO_4) and hydrogen peroxide (H_2O_2) with volume ration of 7:3, was used to clean the substrates. The glass substrates were placed into the piranha solution for 30 minutes after increasing the temperature of solution to 80℃. Spin-coating the substrates with a 2 wt% solution of the fluorosilane (FC-3283) (purchased from 3M company) was applied at a speed of

1000 rpm for 30sec, and followed by baking the substrates at 110℃ for 10min to enhance the coating of Teflon on the substrates. An amorphous flouropolymer, Teflon AF-1601 (6 wt% solution in FC-75), purchased from Dupont, was spin coated onto the substrates at 4000rpm for 40 second, subsequently annealed at 100℃ for 30 min, and followed by an additional 30 min at 225℃. For self-assembly, block copolymer, polystyrene-*block*-poly (4-vinylpyridine) (PS-*b*-P4VP) used in this study without further purification was purchased from Polymer Source (Quebec, Canada, number-average molecular weight M_n^{PS} = 41.5 kg/mol, M_n^{P4vp} = 17.5 kg/mol, molecular weight distribution M_w/M_n=1.07), the structure of which is shown in Figure 25.

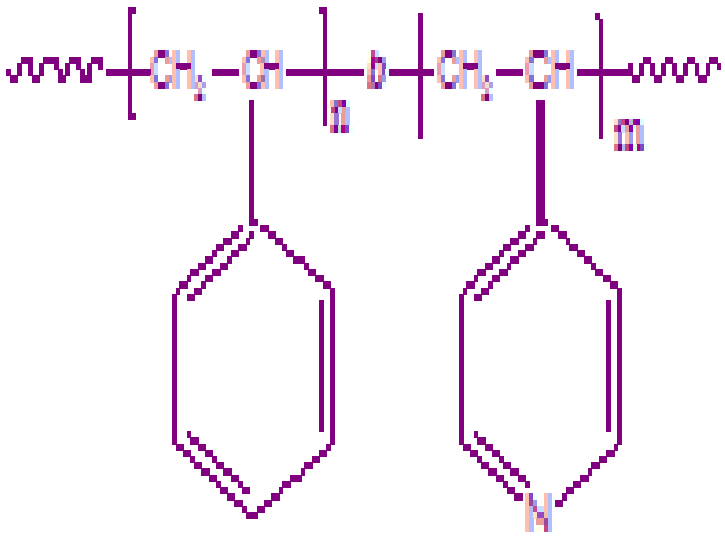

Figure 25. The structure of PS-*b*-P4VP diblock copolymer (Polymer Source).

0.5 wt% polymer solution of PS-*b*-P4VP in toluene/THF (tetrahydrofuran) mixture (a mass ratio of toluene/THF = 7/3) was spin coated at 2000 rpm for 40 seconds onto glass substrates. As-spun polymer films were annealed under THF vapor at room temperature for 3 h to increase the lateral ordering of the films. The solvent annealed PS-*b*-P4VP films were immersed in ethanol for 20 min to create nanoscopic pores. For synthesis of gold dot arrays, 0.3 wt% gold(III) chloride hydrate ($HAuCl_4 \cdot xH_2O$, Aldrich) in ethanol was used. To introduce gold, the solvent annealed copolymer films were immersed in gold solution for 2 min, leading to the incorporation of gold into P4VP phases. The films were then exposed to oxygen plasma to remove organics to form gold nanoparticle arrays

4.2.2 Characterization of morphology and sample

Surface morphology of samples was investigated by using filed emission scanning microscope (FE-SEM: Phillips, XL30 ESEM) and atomic force microscopy (AFM, Model Dimension 3100 (VEECO) Scanning Microscope) in tapping mode and using a VEECO 320 kHz probe. Reactive ion etching (RIE, Oxford Plasmalab 80 RIE) was used for oxygen plasma processing to create Teflon nanopillar arrays. Water droplet contact angles of the samples were measured with the sessile drop method with Video Contact Angle System (KSV Instruments Ldt., CAM 100) equipped with analysis software. A micropipette fabricated from a quartz tube (1.0 mm outside diameter and 0.7 mm inside diameter) by laser heating and tensile stretching using a pipette maker (Sutter Instrumetn Co., P-2000), followed by a hydrophobic coating of

the micropipette surface was used to allow easy transfer of the droplet to the sample surface.

4.3 Results and Discussion

As illustrated in Figure 26, Teflon AF precursor solution was spin-coated onto the glass substrate at 4000 rpm and 40 second, followed by baking on the hot plate. Teflon is one of the most inert polymers, and the wettability of diblock copolymers to the surfaces of the substrate should be sufficient to develop the ordered structure of the copolymers. Wetting of solvent (toluene/THF) for dissolving PS-*b*-P4VP to Teflon thin films is not good, and spin-coated PS-*b*-P4VP solution could not be applied to the surface of Teflon. Prior to spin-coating of PS-*b*-P4VP solution onto Teflon films, oxygen plasma was shortly applied to break and activate the surface of Teflon. PS-*b*-P4VP (0.5 wt%) solution was spin-coated onto the activated surfaces of Teflon and the ordering of PS-*b*-P4VP was enhanced by solvent annealing. RIE process was utilized to create Teflon nanopillar arrays on the glass substrate following introduction of Au nanoparticles into P4PV phase to serve as an etch mask.

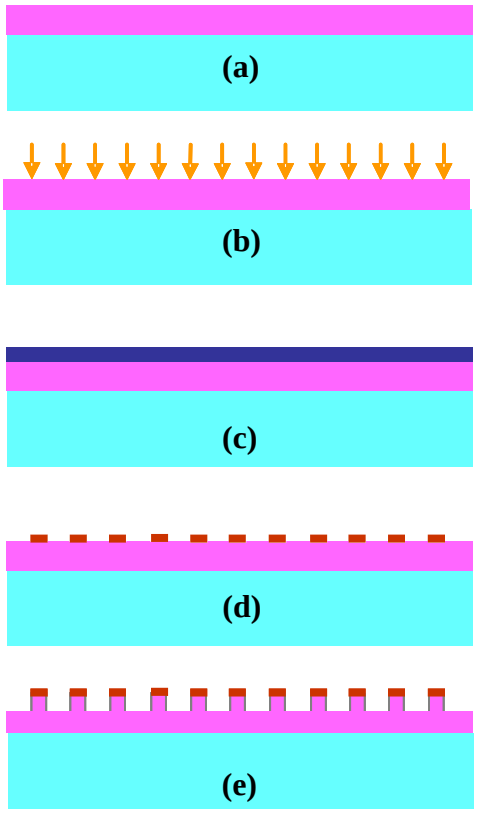

Figure 26. A schematic diagram of Teflon nanopillar arrays. (a) Teflon AF spin-coating on the glass substrate, (b) Oxygen plasma to activate the surface of Teflon films, (c) PS-*b*-P4VP on Teflon & solvent annealing, (d) Au dot arrays, and (e) RIE to make Teflon nanopillar arrays.

Amphiphilic PS-*b*-P4VP with a hydrophobic PS and a hydrophilic P4VP forms uniform micelles in solvents. Here a mixture of toluene and THF was used, which is a favorable solvent for PS blocks, the major component blocks. In solvents, PS-*b*-P4VP forms micelles with PS coronas and P4VP cores. The diameter of micelle and distance between micelles are dependent upon the molecular weight of the P4VP blocks.[71] The morphology and the size of microdomains in PS-*b*-P4VP thin film are affected by the concentration of the toluene/TFH mixture, and increasing THF concentration has induced the transformation in the morphology to cylindrical microdomain oriented normal to the film surface.[72] As-spun thin films have a wide size distribution, resulting in a rather very short-range ordering.[73] To improve long-range hexagonal ordering, various solvent annealing conditions have been used.[73, 74] After improving long-range ordering by solvent annealing, the P4VP phases can be removed by immersing the films in ethanol. This results in the P4VP deposited on the surface of the film, leaving a porous film.[75, 76] In this experiment, solvent of toluene/THF mixture (a mass ratio of toluene/THF = 7/3) for dissolving PS-*b*-P4VP, THF for vapor annealing, and ethanol solvent for inducing a porous film were used. Figure 27 shows AFM images after solvent annealing (Figure 27(a)) and ethanol use (Figure 27(b)). Figure 28 shows SEM image of the porous film on Si substrate. PS-*b*-P4VP (number-average molecular weight M_n^{PS} = 41.5 kg/mol, M_n^{P4vp} = 17.5 kg/mol,) used in this experiment has approximately 20 nm diameter pore sized, porous films.

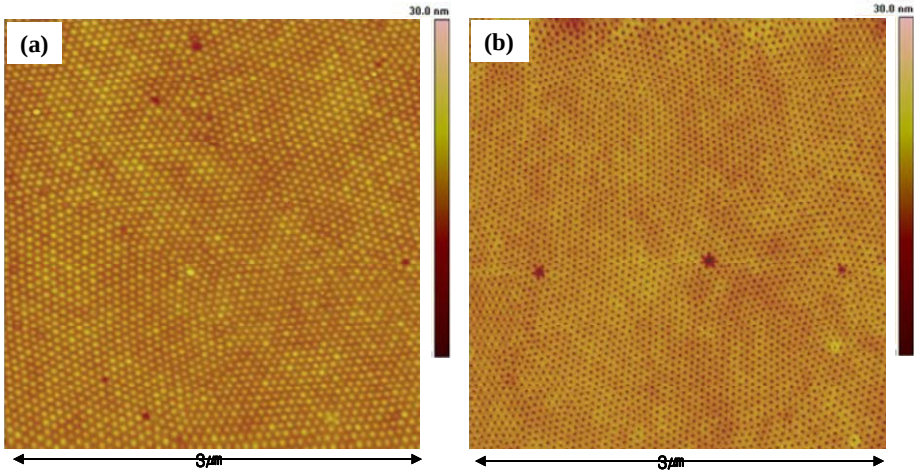

Figure 27. AFM images of PS-*b*-P4VP films. (a) after solvent annealing, and (b) ethanol treatment(porous film).

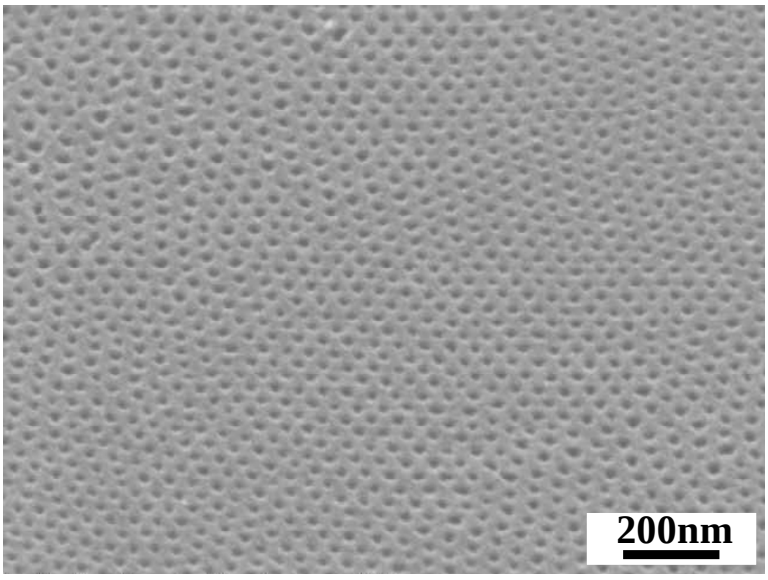

Figure 28. SEM image of porous film of PS-*b*-P4VP.

PS-*b*-P4VP can locally be placed on the P4PV blocks by electrostatic interaction, leading to ordered gold nanoparticle arrays.[59] Immersing PS-*b*-P4VP films into ethanol solution of gold chloride after annealing polymer films resulted in imbedded gold nanoparticles into only P4PV blocks.[77] In this experiment, 0.3 wt% gold(III) chloride hydrate ($HAuCl_4 \cdot H_2O$) in ethanol is used to create gold nanoparticle arrays on the substrate. After solvent annealing of PS-*b*-P4VP films, the film was immersed into the gold solution for 2 min and immediately rinsed with deionized water several times. Ionized gold particles in solvent can deposit only P4VP phase because PS blocks are hydrophobic and P4VP blocks are hydrophilic. Gold nanoparticle arrays can be made by removing only organic parts of PS-*b*-P4VP and gold chloride hydrate by oxygen plasma. Figure 29 shows SEM image of gold nanoparticle arrays on the Si substrate.

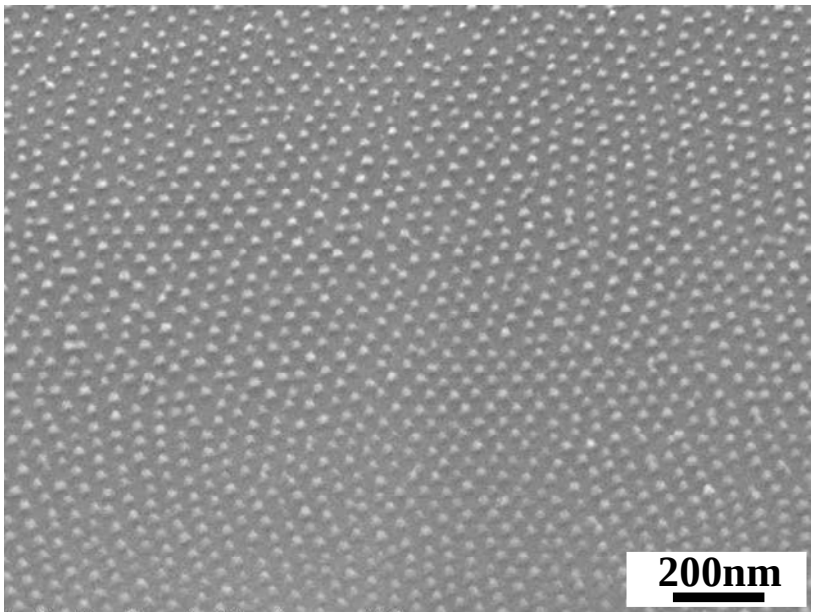

Figure 29. SEM image of gold nanoparticle arrays.

As illustrated in Figure 26, Teflon AF precursor solutions were spin-coated onto the glass substrate followed by oxygen plasma (Pressure: 30mT, Power: 30W, O_2 flow: 20 sccm, and time: 30second) to improve the wettability of PS-*b*-P4VP on the Teflon surface. After PS-*b*-P4VP spin-coating and solvent annealing, ionized gold nanoparticles were introduced into P4VP blocks by means of dipping films into 0.3 wt% gold solution for 2 min. RIE with mixture gasses of O2 and CF4 was used to create Teflon nanopillar arrays with gold nanoparticles serving as an etch mask. Figure 30 shows the SEM image of Teflon nanopillar arrays on the glass substrate. As seen in Figure 30, the height of Teflon pillars is around 160 nm with gold on top of the pillars which was confirmed by energy dispersive X-ray spectroscopy (EDX).

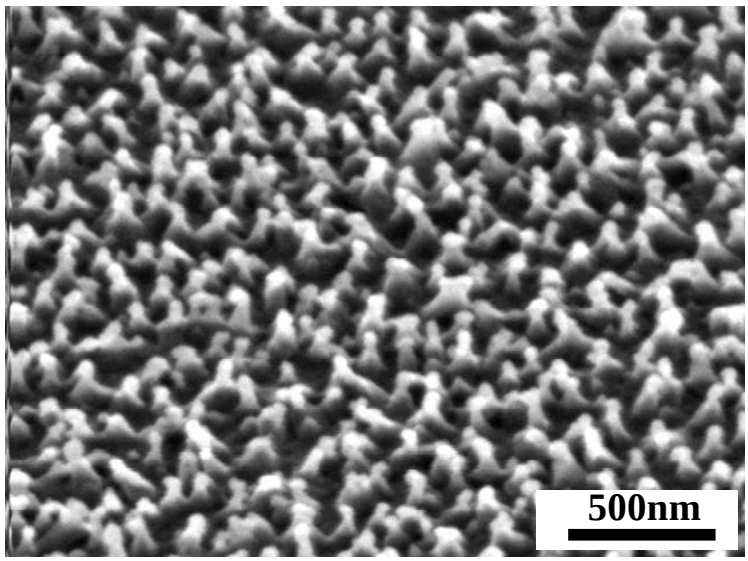

Figure 30. SEM image of Teflon nanopillar arrays on the glass substrate.

For superhydrophobic surfaces, a hydrophobic coating is often required on the surface, especially for naturally hydrophilic surfaces. Fluorinated polymers such as fluoroalkylsilane (FAS) are the most popular chemical for this purpose. Teflon is one of the fluorinated polymers, and the intrinsic contact angle (CA) on the smooth surface was 120^{o}, which is very hydrophobic. Contact angles on Teflon nanopillar arrays were measured without an additional hydrophobic coating. Based on Cassie-Baxter model[2], the apparent CA increases with the small projected area fraction of solid-liquid interface. Pillar structures like seen in Figure 30 have the small projected area fraction, and CA is expected to be a very large value. CA on the Teflon nanopillar arrays in Figure 30 is 168^{o}, which is a superhydrophobic surface. Even gold dots on top of Teflon pillars should themselves be hydrophilic, but CA on Teflon nanopillars has a very high value.

This is probably due to the very small surface area of gold dots that are only located on the top of the hydrophobic Teflon pillars. Figure 31 shows the optical image of a water droplet on the Teflon nanopillar arrays coated the glass, which is optically transparent.

Figure 31. The image of a water droplet on Teflon nanopillar arrays coating on soda lime glass. The insert shows a water droplet contact angle images, which measured the contact angle (168^{o}).

4.4 Summary

In summary, Teflon nanopillar arrays coated on glass have been fabricated by comprising of Teflon coating, PS-*b*-P4VP copolymer, gold nanoparticles embedding into P4VP blocks, and RIE processes. Teflon nanopillars-decorated glass substrate exhibits a very high water droplet contact angle as high as 168^{O}.This method does not need an additional hydrophobic coating because of the hydrophobic property of Teflon itself, which gives optically transparent superhydrophobic glass.

CHAPTER 5: Summary, Conclusions, and Future Work

In summary, Al_2O_3 nanowire topography on a substrate in a vertically aligned configuration has been produced by altering the geometry of as fabricated anodized aluminum oxide pore structures through pore-widening chemical etching. Optimized etching and supercritical CO_2 drying produced very fine ~20–40 nm diameter Al_2O_3 nanowires which exhibit superhydrophobic characteristics, with a very high water droplet contact angle as high as ~169^o. Optically transparent yet highly superhydrophobic glass can be prepared by introducing the aligned Al_2O_3 nanowire structure on the glass surface. Optical property evaluations indicate that such a nanowire-decorated glass substrate exhibits slightly less light transmittance in the UV region but more transmittance in the visible spectrum region when compared to bare untreated glass.

Second, superhydrophobic glass with an extremely high water droplet CA as high as 172^o has been fabricated by the simple methods comprising Ag layer deposition, ball-up heat treatment, and RIE/chemical etching processes. Optically transparent or translucent superhydrophobic glass can be prepared by the different etching methods. In the case of dry etching, nanopillar decorated glass substrates exhibit slightly less light transmittance in the UV regions but more transmittance in the visible spectrum region than bare untreated soda lime glass. Glass substrates fabricated by the chemical etching route give translucent optical properties. Nanopillars themselves are made directly from the glass substrate itself, which means that the structure is very durable and robust.

Finally, Teflon nanopillar arrays coated on glass have been fabricated by Teflon coating, polystyrene-*block*-poly (4-vinylpyridine) (PS-*b*-P4VP) copolymer, gold nanoparticles embedding into P4VP blocks, and RIE processes. Teflon nanopillars-decorated glass substrate exhibits a very high water droplet contact angle as high as 168^{o} .This method does not need an additional hydrophobic coating because of the hydrophobic Teflon property, and gives optically transparent superhydrophobic glass.

The potential applications for superhydrophobic surfaces can be diverse and it is possible that there could be some real materials applications such as window or automobile glass. It is hoped that new fabrication approaches and techniques for superhydrophobic surfaces accomplished in this work contribute to the advancement of materials and applications technology using self-cleaning glass surfaces.

REFERENCES

1. Wenzel, R. N., *Resistance of solid surfaces to wetting by water.* Ing. Eng. Chem., 1936. **28**(8): p. 988-994.

2. Cassie, A. B. D. and S. Baxter, *Wettability of porous surfaces.* Trans. Faraday Soc., 1944. **40**: p. 546-551.

3. Barthlott, W. and C. Neinhuis, *Purity of the sacred lotus, or escape from contamination in biological surfaces.* Planta, 1997. **202**(1): p. 1-8.

4. Cao, L., et al., *Super water- and oil-repellent surfaces on intrinsically hydrophilic and oleophilic porous silicon films.* Langmuir, 2008. **24**(5):p. 1640-1643.

5. Tadanaga, K., N. Katata, and T. Minami, *Formation process of super-water-repellent Al_2O_3 coating films with high transparency by the sol-gel method*. J. Am. Ceram. Soc., 1997. **80**(12): p. 3213-16.

6. Nakajima, A., et al., *Preparation of transparent superhydrophobic boehmite and silica films by sublimation of aluminum acetylacetonate.* Adv. Mater., 1999. **11**(16): p. 1365-1368.

7. Nakajima, A., et al., *Preparation of hard super-hydrophobic films with visible light transmission.* Thin Solid Films, 2000. **376**(1-2): p. 140-143.

8. Suzuki, S., et al., *Hydrophobicity and freezing of a water droplet on fluoroalkylsilane coating with different roughness.* Langmuir, 2007. **23**(17): p. 8674-8677.

9. Coffinier, Y., et al., *Preparation of superhydrophobic silicon oxide nanowire surfaces.* Langmuir, 2007. **23**(4): p. 1608-1611.

10. Xiu, Y., et al., *Hierarchical silicon etched structures for controlled hydrophobicity / superhydrophobicity.* Nano Lett., 2007. **7**(11): p. 3388-3393.

11. Cao, L., et al., *Super water- and oil-repellent surfaces on intrinsically hydrophilic and oleophilic porous silicon films.* Langmuir, 2008. **24**(5): p. 1640-1643.

12. Lau, K. K. S., et al., *Superhydrophobic carbon nanotube forests.* Nano lett., 2003. **3**(12): p. 1701-1705.

13. Jokinen, V., L. Sainiemi, and S. Franssila, *Complex droplets on chemically modified silicon nanograss.* Adv. Mater., 2008. **20**(18): p. 3453-3456.

14. Nishino, T., et al., *The lowest surface free energy based on –CF_3 alignment.* Langmuir, 1999. **12**(13): p. 4321-4323.

15. Bailey, T., et al., *Step and flash imprint lithography: Template surface treatment and defect analysis.* J. Vac. Sci. Technol. B, 2000. **18**(6): p. 3572-3577.

16. Zhang, L., et al., *Superhydrophobic Behavior of a Perfluoropolyether Lotus-Leaf-like Topography*. Langmuir, 2006. **22**(20): p. 8576-8580.

17. Ming, W., et al., *Superhydrophobic Films from Raspberry-like Particles*. Nano Lett., 2005. **5**(11): p. 2298-2301.

18. Sun, C., L. Q. Ge, and Z. Gu, *Fabrication of super-hydrophobic film with dual-size roughness by silica sphere assembly.* Thin Solid Films, 2007. **515**(11): p. 4686-4690.

19. Lee, J. A. and T. J. McCarthy, *Polymer Surface Modification: Topography Effects Leading to Extreme Wettability Behavior*. Macromolecules, 2007. **40**(11): p. 3965-3967.

20. Ma, M., et al., *Decorated Electrospun Fibers Exhibiting Superhydrophobicity.* Adv. Mater., 2007. **19**(2): p. 255-259.

21. Zheng, J., et al., *Studies on the controlled morphology and wettability of polystyrene surfaces by electrospinning or electrospraying.* Polymer, 2006. **47**(20): p. 7095-7102.

22. Tadanaga, K., N. Katata, and T. Minami, *Super-Water-Repellent Al_2O_3 Coating Films with High Transparency.* J. Am. Ceram. Soc., 1997. **80(4):** p. 1040-42.

23. Shirtcliffe, N. J., et al., *Superhydrophobic to superhydrophilic transitions of sol–gel films for temperature, alcohol or surfactant measurement.* Mater. Chem. Phys., 2007. **103**(1): p. 112-117.

24. Hosono, E., et al., *Superhydrophobic Perpendicular Nanopin Film by the Bottom-Up Process.* J. Am. Chem. Soc., 2005. **127**(30): p. 13458-13459.

25. Wang, M. F., N. Raghunathan, and B. Ziaie, *A Nonlithographic Top-Down Electrochemical Approach for Creating Hierarchical (Micro-Nano) Superhydrophobic Silicon Surfaces.* Langmuir, 2007. **23**(5): p**.** 2300-2303.

26. Satyaprasad , A., V. Jain, and S. K. Nema, *Deposition of superhydrophobic nanostructured Teflon-like coating using expanding plasma arc.* Appl. Surf. Sci., 2007. **253**(12): p. 5462-5466.

27. Masuda, H. and M. Satoh, *Fabrication of Gold Nanodot Array Using Anodic Porous Alumina sa an Evaporation Mask.* Jpn. J. Appl. Phys., 1996. **35**(1B): p. L129-L129.

28. Masuda, H., K. Yasui, and K. Nishio, *Fabrication of Ordered Arrays of Multiple Nanodots Using Anodic Porous Alumina as an Evaporation Mask.* Adv. Mater., 2000. **12**(14): p. 1031-1033.

29. Nicewarner-Peña, S. R., et al., *Submicrometer Metallic Barcodes.* Science, 2001. **294**(5540): p. 137-141.

30. Li, Y., et al., *Preparation of Cadmium Sulfide Nanowire Arrays in Anodic Aluminum Oxide Templates.* Chem. Mater., 1999. **11**(12): p. 3433-3435.

31. Gapin, A. I., et al., *CoPt patterned media in anodized aluminum oxide templates.* J. Appl. Phys., 2006. **99**(8): p. 08G902-3.

32. Xiao, Z. L., et al., *Fabrication of Alumina Nanotubes and Nanowires by Etching Porous Alumina Membranes.* Nano Lett., 2002. **2**(11): p. 1293-1297.

33. Yuan, Z., H. Huang, and S. Fan, *Regular Alumina Nanopillar Arrays.* Adv. Mater., 2002. **14**(4): p. 303-306.

34. Thongmee, S., et al., *Aging Time Effect on the Formation of Alumina Nanowires on AAO Template.* Synth. React. Inorg. Met. Org. Chem., 2008. **38**(6): p**.** 469-474.

35. Koponen, H. K., et al., *Modification of cycloolefin copolymer and poly(vinyl chloride) surfaces by superimposition of nano- and microstructures.* Appl. Surf. Sci., 2007. **253**(12): p. 5208-5213.

36. Masuda, H. and K. Fukuda, *Ordered Metal Nanohole Arrays Made by a Two-Step Replication of Honeycomb Structures of Anodic Alumina.* Science, 1995. **268**(5216): p. 1466-1468.

37. Artus, G. R. J., et al., *Silicone Nanofilaments and Their Application as Superhydrophobic Coatings.* Adv. Mater., 2006. **18(20): p.** 2758-2762.

38. Bravo, J., et al., *Transparent Superhydrophobic Films Based on Silica Nanoparticles.* Langmuir, 2007. **23**(13): p. 7293-7298.

39. Shang, H. M., et al., *Nanostructured superhydrophobic surfaces.* J. Mater. Sci., 2005. **40**(13): p. 3587-3591.

40. Tripp, C. P. and M. L. Hair, *Reaction of Methylsilanols with Hydrated Silica*

Surfaces: The Hydrolysis of Trichloro-, Dichloro-, and Monochloromethylsilanes and the Effects of Curing. Langmuir, 1995. **11**(1): p. 149-155.

41. Ishizaki, T., et al., *Fabrication and characterization of ultra-water-repellent alumina–silica composite films.* J. Phys. D: Appl. Phys., 2007. **40**(1): p**.** 192-197.

42. Zhang, X., et al., *Thermal stability of the structural features in the superhydrophobic boehmite films on austenitic stainless steels.* Appl. Surf. Sci., 2008. **254**(16): p. 5129-5133.

43. Nakajima, A., et al., *Transparent Superhydrophobic Thin Films with Self-Cleaning Properties.* Langmuir, 2000. **16**(17): p. 7044-7047.

44. Ran, C., et al., *Wetting on Nanoporous Alumina Surface: Transition between Wenzel and Cassie States Controlled by Surface Structure.* Langmuir, 2008. **24**(18): p. 9952-9955.

45. Chu, S. Z., et al., *Formation and Microstructures of Anodic Alumina Films from Aluminum Sputtered on Glass Substrate.* J. Electrochem. Soc., 2002. **149**(7): p. B321-B327.

46. Peng, K. Q., et al., *Synthesis of Large-Area Silicon Nanowire Arrays via Self-Assembling Nanoelectrochemistry.* Adv. Mater., 2002. **14**(16): p. 1164-1167.

47. Peng, K. Q., Huang, Z. P. Huang, and J. Zhu, *Fabrication of Large-Area Silicon Nanowire p-n Junction Diode Arrays.* Adv. Mater., 2002. **16**(1): p. 73-76.

48. Peng, K. Q., et al., *Uniform, Axial-Orientation Alignment of One-Dimensional Single-Crystal Silicon Nanostructure Arrays.* Angew. Chem. Int. Ed., 2005. **44**(18): p. 2737-2742.

49. Qu, Y., et al., *Electrically Conductive and Optically Active Porous Silicon Nanowires.* Nano Lett., 2009. **9**(12): p. 4539-4543.

50. Shen, L., J. Ji, and J. Shen, *Silver Mirror Reaction as an Approach to Construct Superhydrophobic Surfaces with High Reflectivity.* Langmuir, 2008. 24(18): p. 9962-9965.

51. Chen, W., et al., *Ultrahydrophobic and Ultralyophobic Surfaces: Some Comments and Examples.* Langmuir, 1999. **15**(10): p. 3395-3399.

52. Fadeev, A. Y. and T. J. McCarthy, *Trialkylsilane Monolayers Covalently*

Attached to Silicon Surfaces: Wettability Studies Indicating that Molecular Topography Contributes to Contact Angle Hysteresis. Langmuir, 1999. **15**(11): p. 3759-3766.

53. Bates, F. S. and P. M. Harrison, *Block Copolymer Thermodynamics: Theory and Experiment.* Annu. Rev. Phys. Chem., 1990. **41**(1): p. 525-557.

54. Morkved, T. L., et al., *Local Control of Microdomain Orientation in Diblock Copolymer Thin Films with Electric Fields.* Science, 1996. **273**(5277): p. 931-933.

55. Thurn-Albrecht, T., et al., *Nanoscopic Templates from Oriented Block Copolymer Films.* Adv. Mater., 2000. **12**(11): p. 787-791.

56. Segalman, R. A., H. Yokoyama, and E. Kramer, *Graphoepitaxy of Spherical Domain Block Copolymer Films.* Adv. Mater., 2001. **13**(15): p. 1152-1155.

57. Guarini, K. W., C. T. Black, and S. H. I. Yeung, *Optimization of Diblock Copolymer Thin Film Self Assembly.* Adv. Mater., 2002. **14**(18): p. 1290-1294.

58. Blake, A. J., et al., *Inorganic crystal engineering using self-assembly of tailored building-blocks*. Coordination Chemistry Reviews, 1999. **183**(1): p. 117-138.

59. Spatz, J. P., et al., *Ordered deposition of inorganic clusters from micellar block copolymer films.* Langmuir, 2000. **16**(2): p. 404-415.

60. Lu, J., et al., *Fabrication of ordered catalytically active nanoparticles derived from block copolymer micelle templates for controllable synthesis of single-walled carbon nanotubes.* Journal of Physical Chemistry B, 2006. **110**(13): p. 6655-6660.

61. Mansky, P., et al., *Controlling polymer-surface interactions with random copolymer brushes.* Science, 1997. **275**(5305): p. 1459-1460.

62. Thurn-Albrecht, T., J. DeRouchey, and T. P. Russell, *Overcoming interfacial interactions with electric fields.* Macromolecules, 2000. **33**(9): p. 3250-3253.

63. Stoykovich, M. P., et al., *Directed assembly of block copolymer blends into nonregular device-oriented structures.* Science, 2005. **308**(5727): p. 1442-1446.

64. Zhang, J., J. Li, and Y. Han, *Superhydrophobic PTFE surfaces by extension.* Macromol. Rapid Commun., 2004. **25**(11): p. 1105-1108.

65. Daoud, W. A., et al., *Pulsed laser deposition of superhydrophobic thin Teflon films on cellulosic fibers.* Thin Solid Films, 2006. **515**(2): p. 835-837.

66. Campbell, J. L., et al., E*lectrowetting of superhydrophobic ZnO nanorods*. Langmuir, 2008. **24**(9): p. 5091-5098.

67. Choi, C. H. and C. J. Kim, *Large slip of aqueous liquid flow over a nanoengineered superhydrophobic surface.* Phys. Rev. Lett., 2006. **96**(6): p. 96:066001.

68. Biswas, L., et al., *Controlled generation of Ni nanoparticles in the capping layers of Teflon AF by vapor-phase tandem evaporation.* Nano Lett., 2003. **3**(1): p. 69-73.

69. Shiu, J. -Y. and Chen, P. L., *Addressable protein patterning via switchable superhydrophobic microarrays.* Adv. Funct. Mater., 2007. **17**(15): p. 2680-2686.

70. Deng, T., et al., *Micropatterning of block copolymer solutions.* Langmuir, 2002. **18**(18): p. 6719-6722.

71. Antonietti, M, et al., *Determination of the micelle architecture of polystyrene/ poly(4-vinylpyridine) block copolymers in dilute solution.* Marcromolecules, 1994. **27**(12): p. 3276-3281.

72. Park, S., et al., *Solvent-induced transition from micelles in solution to cylindrical microdomains in diblock copolymer thin films.* Macromolecules, 2007. **40**(25): p. 9059-9063.

73. Kim, B., et al., *Fabrication of ordered anodic aluminum oxide using a solvent-induced array of block-copolymer micelles.* Small, 2007. **3**(11): p. 1869-1872.

74. Zhao, J., et al., *Study of the time evolution of the surface morphology of thin asymmetric diblock copolymer films under solvent vapor*. Polymer, 2005. **46**(17): p. 6513-6521.

75. Meister, A. et al., *Local modification of micellar layers using nanoscale dispensing*. Microelectron. Eng., 2006. **83**(4-9): p. 1509-1512.

76. Park, S., et al., *Fabrication of highly ordered silicon oxide dots and stripes from block copolymer thin films*. Adv. Mater., 2008. **20**(4): p. 682-685.

77. Sohn, B. H. and B. H. Seo, *Fabrication of the multilayered nanostructure of alternating polymers and gold nanoparticles with thin films of self-assembling diblock copolymers.* Chem. Mater., 2001. **13**(5): p. 1752-1757.